Journal of proteome research

Article

pubs.acs.org/jpr

p63 Isoforms Regulate Metabolism of Cancer Stem Cells

Simona D'Aguanno,[†,‡] Daniela Barcaroli,[†,§] Claudia Rossi,[†,§] Mirco Zucchelli,[†,§] Domenico Ciavardelli,[§,#] Claudio Cortese,[‡,∥] Antonella De Cola,[†,§] Silvia Volpe,[⊥] Daniela D'Agostino,[†,§] Matilde Todaro,[⊥] Giorgio Stassi,[⊥] Carmine Di Ilio,[†,§] Andrea Urbani,*[,‡,∥,▽] and Vincenzo De Laurenzi*[,†,§,▽]

[†]Department of Experimental and Clinical Sciences, "G. d'Annunzio University", Via dei Vestini 31, Chieti-Pescara 66100, Italy

[‡]Fondazione Santa Lucia-IRCSS, Via Ardeatina 306, Rome 00142, Italy

[§]Centre of Study on Aging (Ce.S.I.), "G. d'Annunzio" University Foundation,Via dei Vestini 31, Chieti 66100, Italy

[∥]Department of Experimental Medicine, University of Rome "Tor Vergata", Via Montpellier 1, Rome 00133, Italy

[⊥]Department of Surgical and Oncological Sciences, University of Palermo, Via del Vespro 129, Palermo 90100, Italy

[#]University of Enna "Kore", Via delle Olimpiadi, Enna 94100, Italy

Supporting Information

ABSTRACT: p63 is an important regulator of epithelial development expressed in different variants containing (TA) or lacking (ΔN) the N-terminal transactivation domain. The different isoforms regulate stem-cell renewal and differentiation as well as cell senescence. Several studies indicate that p63 isoforms also play a role in cancer development; however, very little is known about the role played by p63 in regulating the cancer stem phenotype. Here we investigate the cellular signals regulated by TAp63 and ΔNp63 in a model of epithelial cancer stem cells. To this end, we used colon cancer stem cells, overexpressing either TAp63 or ΔNp63 isoforms, to carry out a proteomic study by chemical-labeling approach coupled to network analysis. Our results indicate that p63 is implicated in a wide range of biological processes, including metabolism. This was further investigated by a targeted strategy at both protein and metabolite levels. The overall data show that TAp63 overexpressing cells are more glycolytic-active than ΔNp63 cells, indicating that the two isoforms may regulate the key steps of glycolysis in an opposite manner. The mass-spectrometry proteomics data of the study have been deposited to the ProteomeXchange Consortium (http://proteomecentral.proteomexchange.org) via the PRIDE partner repository with data set identifiers PXD000769 and PXD000768.

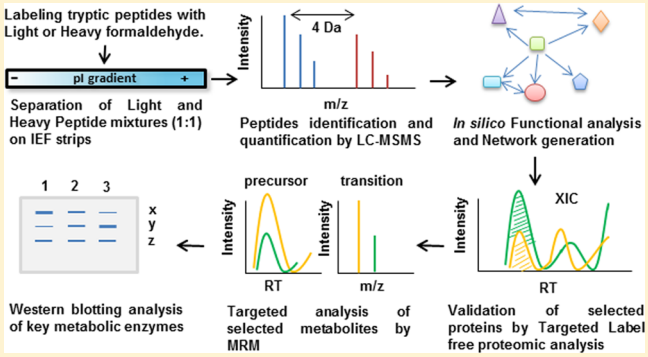

KEYWORDS: *p63, colon cancer stem cells, proteomics, stable isotope dimethyl labeling, glucose metabolism*

INTRODUCTION

The p53/p63/p73 family is composed of strictly related transcription factors sharing highly homologous sequences. Thus it was supposed for a long time that these proteins could also share functional roles.[1,2] In recent years, distinct roles for each member have emerged on the basis of new experimental evidence. A huge number of studies demonstrated that p53 is a master tumor suppressor gene, whose mutation is frequently associated with cancer,[3] while the role of p63 in tumor suppression still needs more clarification. The study of the role played by p63 is sometimes rendered more problematic by the structural variability of protein products originating from p63 gene. Similarly to p73, p63 gene is transcribed in multiple isoforms. The amino-terminal region of p63 may include an acidic transactivation domain (TA isoforms) or lack this domain (ΔN isoforms).[4] Moreover alternative splicing may originate different transcripts responsible for variability at protein carboxy-terminals, thus bringing about α, β, γ, δ, and ε variants. From a structural point of view, p63α is closer to p73α, sharing a common sterile alpha motive (SAM) domain, absent in p53. TAp63 and ΔNp63 regulate to different extent the expression of their targets, which are involved in several cellular functions such as apoptosis, cell cycle arrest, and senescence.[4,5]

Altered levels of p63 were demonstrated in different epithelial tumors, such as in breast, head and neck, and lung, by the use of targeted detection techniques, such as PCR, or by using antibodies, which could not discriminate among TAp63 and ΔNp63, thus sometimes giving controversial results.[6] In particular, these studies showed that the TA isoforms are not expressed or weakly expressed, whereas the ΔN isoforms are expressed at higher levels.[6,7] Conversely to p53, mutations of p63 are extremely rare in tumors.[7] The expression pattern showed by the different isoforms observed in cancer is consistent with the concept that TAp63α may function as

Received: December 18, 2013
Published: March 5, 2014

   dx.doi.org/10.1021/pr4012574 | J. Proteome Res. 2014, 13, 2120−2136

Scheme 1. Workflow Diagram Showing the Experimental Design

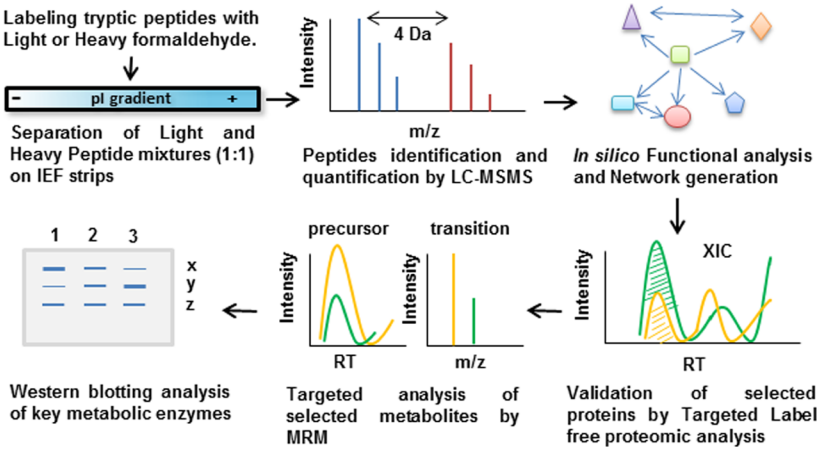

tumor suppressor, while ΔNp63α may act as an oncogene, antagonizing p53, TAp63, and TAp73, by affecting the expression of those target genes, which are generally under their control;[8] this, however, is probably an oversimplified vision of how these transcription factors work, and indeed ΔNp63 contains an additional transactivation domain and has been shown to up-regulate expression of a specific set of genes.[8] Evaluation of p63 expression profile also revealed in a few cases the lack of the ΔNp63 protein in human tumors such as diffuse large B-cell lymphoma (DLBCL), suggesting that this isoform may also acts as a tumor suppressor.[9] The epithelial mesenchymal transition (EMT), a relevant process involved in cancer cell metastasis as well as in embryogenesis, is also known to be modulated by ΔNp63. As an example, it was reported in a model of squamous cell carcinoma (SCC) that during EMT, SNAIL, a regulator of cellular invasiveness, down-regulates ΔNp63 expression and in parallel also down-regulates E-cadherin.[10] Recently, experiments conducted in prostate cancer cells showed that both TAp63 and ΔNp63 isoforms regulate expression of miR-205, which is essential for p63 to explain its inhibitory effect on EMT.[11] In vitro and in vivo experiments revealed that TAp63 is a suppressor of tumorigenesis and metastasis.[12] According to the proposed model, TAp63 transcriptionally activates metastasis suppressor genes or microRNAs, such as DICER1, mir-130b, and BHLHE41, also known as SHARP1, and genes involved in integrin recycling. The suppression of the metastasis mediated by TAp63 is inhibited by aggregation with mutant p53 and by transforming growth factor-β (TGFβ).[8,12] p63 was also reported to be involved in cancer chemosensitivity.[5] Endogenous TAp63 expression was increased after drug treatment in hepatoma cells, and the abrogation of TAp63 function caused enhanced chemoresistance. These observations were in accordance with the pro-apoptotic activity of TAp63, carried out through death receptor- and mitochondrial-mediate apoptosis pathway.[13] On the contrary, ΔNp63 does not show pro-apoptotic activity but can compete with TAp63 for the same responsive element, thus inhibiting the TAp63-mediated apoptotic program.[14]

A large plethora of experimental research regarding p63 function focused not only on its involvement in cancer but also on characterizing its pivotal role in epithelial development.[5] Mutant mice that do not express p63 are born lacking limbs as well as skin and its appendages[15,16] and have markedly abnormal prostate and bladder epithelia.[17] More deepen understanding about the distinct functions of the two isoforms, achieved by the characterization of knockout mice for TA and ΔNp63 isoforms, revealed that these anomalies result from the lack of ΔNp63.[18] ΔNp63 is expressed in basal epithelial cells and is required for normal development of several epithelial tissues, including the bladder, prostate glands and colorectal epithelia.[19] This isoform is necessary for stem-cell renewal[15,20] as well as for terminal differentiation,[18,21] whereas TAp63 is implicated in maintaining stem cells in quiescence and preventing premature aging[22] and senescence.[12,22] Because of its implication in both cancer and stemness, p63 may also play a relevant role in maintaining the cancer stem-cell phenotypes, particularly in tumors of epithelial origin.[6,14,23] Colorectal tumors are hierarchically organized with a minor cancer stem cells (CSCs) niche, showing self-renewal and multilineage differentiation capacity, responsible for the formation of more differentiated less malignant cells, making up the bulk of the tumor.[24,25] CSCs have also been implicated in drug resistance and tumor recurrence, although the nature of this relationship is only beginning to be clarified.[26] Onco-proteomics may significantly contribute to explore this field, employing sensitive methodological approaches and accurate procedures to characterize proteins involved in the cellular processes responsible for maintaining the CSC pool.[27]

In this work, we investigated the effects of TAp63α and ΔNp63α overexpression in colon CSCs, which express a low level of the endogenous isoforms by complementary proteomics approaches (Scheme 1). In the discovery phase, we carried out a quantitative proteome analysis by stable isotope dimethyl labeling to define the expression profiles of the infected cells, generating raw data for unsupervised data-mining of functional biological processes. Then, in a subsequent validating phase, we employed a targeted analysis, at both protein and metabolite levels, focusing, in particular, on metabolic processes. This experimental design allowed us to obtain an overview on cellular pathways modulated by p63, thereby offering the opportunity to better understand its implication in maintaining the CSCs phenotype.

EXPERIMENTAL PROCEDURES

Purification and Culture of CSCs

Human colon tissue fragments were obtained in accordance with the ethical standards of the institutional committee on human experimentation from a patient undergoing a colon

dx.doi.org/10.1021/pr4012574 | J. Proteome Res. 2014, 13, 2120−2136

resection for colon adenocarcinoma. Histological diagnosis was based on microscopic features of carcinoma cells determining the histological type and grade. Cancer tissues were extensively washed in saline buffer containing antibiotics and incubated overnight in DMEM/F12 (1:1) containing penicillin (500 IU/mL), streptomycin (500 μg/mL) and amphotericin B (1.25 μg/mL). Enzymatic digestion was performed using collagenase (1.5 mg/mL) and hyaluronidase (20 μg/mL) in DMEM containing antibiotics/antimycotics for 1 h. Recovered cells were then cultured in serum-free medium DMEM/F12 (1:1) supplemented with 6 mg/mL glucose, 1 mg/mL $NaHCO_3$, 5 mM HEPES, 2 mM L-glutamine, 4 μg/mL heparin, 4 mg/mL BSA, 10 ng/mL βFGF, 20 ng/mL EGF, 100 μg/mL transferrin sodium salt, 25 μg/mL insulin, 9.6 μg/mL putrescine, 30 nM sodium selenite, and 20 nM progesterone to a final concentration of 3×10^5 cells/mL at 37 °C in a humidified atmosphere of 5% (v/v) CO_2 in air. These culture conditions select for immature tumor cells that slowly proliferate, giving rise, within 2 to 3 months, to tumor cell aggregates, called "spheres".[28]

Plasmids

TAp63α-Tween and ΔNp63α-Tween expression vectors were generated from TAp63α−pcDNA and ΔNp63α−pcDNA constructs, kindly provided by Prof. G. Melino, University of Rome "Tor Vergata", Roma, Italy.[29] Inserts were subcloned into XbaI-XhoI unique sites of Tween lentiviral vector[30] under the control of hCMV promoter. This vector constitutively expresses GFP under the control of hPGK promoter.

Lentiviral Trasduction and Flow Cytometry

Lentiviral supernatants were produced by transient cotransfection of a three-plasmid expression system in the packaging 293T cell line, using the calcium phosphate transfection kit (K2780-01, Invitrogen). The calcium phosphate−DNA precipitate was removed after 9 h by washing once in PBS and replacing the medium. Viral supernatant was collected 48 h after transfection, filtered through 0.45 μm pore nitrocellulose filter. CSCs were plated in a six-well plate in the presence of viral supernatant and 4 μg/mL of polybrene. Plates were centrifuged for 45′ at 1800 revolutions/min and incubated at 37 °C for 75′ in a 5% CO2 incubator. Cells were then washed twice and replated in fresh medium.[31] Transduction efficiency was assessed as the percentage of GFP-positive cells measured by flow cytometry (FACSCanto II Instrument, BD Biosciences) 48 h postinfection. Data were analyzed with CELLQuest software (BD Biosciences).

Peptides Labeling

Cells of three independent infection experiments for each condition were lysed by sonication, and total proteins were extracted in 6 M urea, 100 mM Tris/HCl pH 7.5 buffer. Protein concentration was determined by the Bio-Rad Protein Assay (Bio-Rad Laboratories, Hercules, CA). 50 μg for each of the three protein extractions was pooled for condition, precipitated by the addition of a mix of ethanol, methanol, and acetone (ratio 2:1:1, v/v/v) and solubilized in 6 M urea, 100 mM TEAB pH 8.5, a buffer compatible with subsequent dimethylation.[32] 25 μL of 6 M urea, 100 mM TEAB pH 8.5, containing 100 μg of pooled protein extract was reduced and alkylated by adding DTT (10 mM) (1 h at 36 °C) and iodoacetamide (50 mM) (1 h at RT). Protein samples were digested with 1:20 (w/w) sequence grade trypsin (Promega, Madison, WI) at 36 °C overnight. Tryptic peptides were subjected to chemical labeling by modifying the already published protocol.[32,33] Stable isotope dimethyl labeling was achieved by the reaction of peptide primary amines (the N terminus and the side chain of lysine residues) with formaldehyde to generate a Schiff base, rapidly reduced by adding cyanoborohydride to the tryptic digestion. Light labeled peptides were obtained by using formaldehyde-D_0 and cyanoborohydride, which produced a mass increase of 28 Da, while the use of deuterated formaldehyde (formaldehyde-D_2) generated a mass increase of 32 Da, achieving the heavy labeled samples. The labeled samples can then be mixed because the different isotopes do not affect the behavior of the labeled peptides in LC−MS/MS. An insignificant isotopic effect in chromatography runs has been verified by Hsu at colleagues[33] and by other subsequent dedicated studies,[34] so that the coelution of paired labeled peptides (the pair of heavy and light peptide) is expected to occur.

In MS, the different stable isotopically labeled peptides can be recognized by the known mass difference between them. Finally, quantification can be performed by comparing the signal intensity of the differentially labeled peptides. In detail: 1.5 μL of formaldehyde-D_0 (20% in water) was mixed in the peptides mixture, vortexed, and incubated for 5 min at RT. Then, 2.5 μL of freshly prepared sodium cyanoborohydride (1 M) was added and allowed to react for 1 h at RT. Deuterium labeling was performed by similar procedure but by using formaldehyde-D_2 (20% in water). An extensive characterization of dimethylation in quantitative analysis has been recently performed by our group,[35] demonstrating, in accordance with other published works,[32,33] that this approach is cheap, quick, and applicable to any sample, including complex samples. The completion of the reaction was evaluated by running singularly the D_0- and D_2-labeled samples in nL−MS/MS by using a Q-Tof Premier mass spectrometer (Waters, Manchester, U.K.) operating in DDA mode.[36] In the case of complete D_0 or D_2 reaction, it is expected that all peptides will be dimethylated (at N-terminus) or tetramethylated (both at N-terminus and at the side chain of lysine residue). By including dimethylation at the N-terminus and side chain of lysine residue as a variable modification in the database search, all peptides of D_0- and D_2-labeled samples were found to be modified (representative database search results were reported in Supplementary Table 1S in the Supporting Information). On the contrary, when these modifications were not applied, we did not obtain peptide identification.

Light and heavy labeled samples were mixed 1:1 prior to peptide separation by isoelectric focusing. We analyzed TAp63-D_0 with CTRL-D_2 (1:1) and ΔNp63-D_0 with CTRL-D_2 (1:1). The inverted labeled samples were also mixed: TAp63-D_2 with CTRL-D_0 (1:1) and ΔNp63-D_2 with CTRL-D_0 (1:1).

Immobilized pH Gradient Isoelectric Focusing (IPG-IEF) Separation of Labeled Peptides

Mixed samples of light and heavy labeled peptides were separated by IPG-IEF prior to mass spectrometry analysis.[37−39] A solution of 8 M urea, 0.5% (v/v) IPG-buffer (pH 3−10 NL, Amersham Biosciences, Buckinghamshire, U.K.), and bromophenol blue in traces was added to the mixture of labeled peptides until a final volume of 350 μL. Isoelectric focusing was performed in an IPGphor system (Amersham Biosciences) using Immobiline Dry strips 18 cm, pH interval 3−10 nonlinear at 20 °C. After 8 h of passive and 8 h of active rehydration at 30 V, peptides were focused ramping to 300 V over 2 h, holding at

300 V for 1 h, ramping to 3500 V over 3 h, holding at 3500 V for 3 h, successively ramping to 8000 V over 3h and plateau at 8000 V until 50 000 V/h.

nLC−MS/MS Analysis

Focused strips were cut into 15−17 pieces, and peptides were extracted twice with a solution of 0.1% formic acid (FA) and 50% acetonitrile (1:1) and then with 100% acetonitrile, collecting supernatants into autosampler vials. The extracted mixtures were dried by Speed-Vac and dissolved in 20 μL of 0.1% FA. Five microliters of each sample was separated by a Proxeon Easy-nLC II (Thermo Scientific, Waltham, MA) chromatographic system equipped with an EASY-Column C18, 5 μm, 100 μm × 20 mm precolumn (Thermo Scientific) and using an Acclaim PepMap100 C18, 5 μm, 75 μm × 25 mm (Dionex, Thermo Scientific) nanoscale LC column. Mobile phase A was water with 0.1% FA, and mobile phase B was 0.1% FA in acetonitrile. Peptides were separated with a reverse-phase gradient of 5−35% mobile phase B over 57 min at a flow rate of 300 nL/min and a rinse with 100% mobile phase B for 10 min. The chromatographic system was coupled online to a MicrOTOF Q-II mass spectrometer (Bruker-Daltonics, Bremen, Germany) equipped with an ESI nanosprayer ion source. During acquisition, source settings were: end plate offset: −500 V; capillary = 4500 V; nebulizer = 0.4 bar; dry gas = 4 L/min; dry temperature = 160 °C.

Spectra acquisition in the mass range 400−1400 m/z was performed by using an Auto (MS/MS) mode method optimized for quantitative proteomics (Bruker-Daltonics, Bremen, Germany), setting MS spectra rate to 1.0 Hz and the number of precursor ions to 5, using active exclusion after two spectra, using Argon in collision gas cell, and selecting the SILE option. By this option, it is possible to define the delta mass introduced by the labeling approach. A delta mass of 4 Da indicates the N-terminal dimethylation, while a delta mass of 8 Da indicates the dimethylation of both N-terminal and lysine residue of the peptide sequence, and thus in the SILE option we specified delta mass = 4.0251; maximum number of labels = 2; and charge range = 1−3.

Peptide Identification and Quantification

Spectra were processed by using Mascot Distiller v2.4.3.3 using the default processing methods optimized for Q-TOF instrument. Peptide identification was achieved by the in-house version of Mascot algorithm (version 2.4), interrogating Swiss-Prot database (released version 2013_02) restricted to *Homo sapiens* taxonomy (20 248 sequences). Search parameters were: carbamidomethylation of cysteines as fixed modification, oxidation of methionines as variable modification, dimethylation as quantitation method, one missing cleavage allowed on tryptic peptides, 20 ppm for peptide tolerance, 0.1 Da for fragment tolerance, p value < 0.05 for peptide significant value of identification, and decoy option active. Proteins identified with one unique peptide were manually validated. After protein identification, only peptides matching the following criteria were included in the final quantitation analysis: p value < 0.05 for peptide significant value, bold red, unique sequences, standard error <0.2, correlation threshold >0.9, and fraction threshold of at least 0.5. Because the fit between the experimental and the calculated peaks is never perfect, Distiller allows us to accept a peptide ratio by applying the threshold of three measures of the quality of the fit: standard error, fraction, and correlation. The standard error is the estimated error for the calculated ratio. The correlation coefficient, which considers the shape of the peak distribution, is the estimation of the good fit between the predicted and observed precursor isotope distributions. Fraction is the fraction of the precursor region accounted for by the expected precursor peaks. The resulting quantified proteins were reported in the quantitation report, where the protein ratio type selected was "median" and the interval of confidence was expressed as geometric standard deviation, SD(geo), which is a factor, not a difference. Finally, only proteins with a ratio >1.3 or <0.7 and Mascot score above 40 and acceptable SD(geo) were considered in the further analysis. Proteins were identified with FDR < 1%. The mass spectrometry proteomics data have been deposited to the ProteomeXchange Consortium (http://www.proteomexchange.org) via the PRIDE partner repository[40,41] with the data set identifier PXD000768 and DOI: 10.6019/PXD000768 for TAp63 and PXD000769 and DOI: 10.6019/PXD000769 for ΔNp63. These data sets are formally associated with the B/D-HPP initiative on Cancer and Mitochondria.

Bioinformatics Analysis

Modulated proteins identified by proteomic analysis were further analyzed by the PANTHER Classification System (http://www.pantherdb.org), by The Database for Annotation, Visualization and Integrated Discovery (DAVID) (http://david.abcc.ncifcrf.gov/), and by Ingenuity Pathway Analysis software v.8.8 (IPA). Using PANTHER resource, it is possible to categorize genes by their molecular functions or biological processes on the basis of published papers and by evolutionary relationships to predict function when experimental evidence is missing. DAVID provides a comprehensive set of functional annotation tools for investigators to understand biological meaning behind a large list of genes/proteins. IPA highlights protein networks or pathways starting from a continuous updated database of known protein−protein interactions based on direct (physical) and indirect (functional) associations. The algorithm gives back a probability score for each possible network. Scores of 10 or higher (negative log of the p value) have a high confidence of not being generated by random chance alone.[42−44]

Targeted Label-Free Quantitative Analysis

Protein extracts samples were prepared as previously described. Tryptic peptide mixtures of the three different conditions, obtained by in-solution digestion as already described, were separately analyzed by nanoACQUITY UPLC System (Waters, Milford, MA) coupled to a Q-Tof Premier mass spectrometer (Waters, Manchester, U.K.) operating in high-low mode.[42−44] The triplicate of each condition was run. Prior to loading, a digestion of Enolase (ENO1) from *Saccharomyces cerevisiae* (Waters) was added to the sample as an internal standard to have a final concentration of 100 fmol/μL on column. A total of 0.6 μg of protein digestion was injected onto symmetry C18 5 μm, 180 μm × 20 mm as precolumn (Waters) for preconcentration and desalting and separated using a NanoEase BEH C18 1.7 μm, 75 μm × 25 cm nanoscale LC column (Waters) maintained at 35 °C. Mobile phase A was water with 0.1% formic acid, while mobile phase B was 0.1% formic acid in acetonitrile. Peptide separation was obtained by a gradient of 3−40% B over 150 min at flow rate of 250 nL/min, followed by a gradient of 40−90% B over 5 min and a 15 min rinse with 90% B. The Q-Tof Premier mass spectrometer was operated in "Expression Mode" switching between low (4 eV) and high (15−40 eV) collision energies with a scan time of 0.8 s over 50−1990 m/z mass range. Continuum LC−MS data were

dx.doi.org/10.1021/pr4012574 | J. Proteome Res. 2014, 13, 2120−2136

processed and searched using ProteinLynx GlobalServer v2.4 (PLGS) (Waters). Protein identifications were obtained with the embedded ion accounting algorithm of the software and by searching a UniProtKB/SwissProt human database. Parameters for the database search were: automatic tolerance for precursor ions, automatic tolerance for product ions, minimum of three fragment ions matched per peptide, minimum of seven fragment ions matched per protein, minimum of two peptides matched per protein, one missed cleavage, carbamidomethylation of cysteine and oxidation of methionine as modifications, and the false positive rate (FPR) of the identification algorithm <1%.

Acquired raw data were used as input files by Skyline open-source software to perform quantitative analysis.[46,47] A peptide MS/MS spectral library of samples was created from a csv file generated by PLGS software including peptide and fragment ions information. Duplicate or repeated peptides and peptides without a matching protein in the background proteome, the UniProtKB/Swiss-Prot database restricted to *Homo sapiens* taxonomy, were automatically removed. Raw data from single sample runs were processed to generate the eXtracted Ion Chromatogram (XIC) of selected peptide masses. Automatic peak assignment and retention times were verified manually. After Savitzky–Golay smoothing, the peaks corresponding to the precursor ion retention times were integrated and the resulting peak areas were normalized to the endogenous actin and then multiplied by a normalization factor of 100. The normalized peak area was averaged across all acquisitions, and a ratio was generated. p value was calculated by applying Student's t-test.

Metabolomics Analysis

100 μL of a mixture of ethanol/water 80:20 was added to ~5×10^6 cell pellets. Pellets were obtained by pooling cells of three independent infection experiments. Cells were sonicated for 20 min; then, samples were centrifuged (25 000g, 4 °C, 20 min). Supernatants were analyzed by an LC–MS/MS system consisting of a Waters Alliance HT 2795 HPLC separation module coupled to a Waters Quattro Ultima Pt ESI tandem quadrupole mass spectrometer (Waters). The instrument was operated in negative electrospray ionization mode using MassLynx v. 4.0 software (Waters), and data processing was performed using QuanLynx software (Waters). For HPLC analysis, the Atlantis HILIC silica 3 μm 2.1 × 150 mm column (Waters) was used. Thirty μL of the extracted samples was injected onto the HPLC–MS/MS system. The technical replicate was performed. The mobile phase comprised a binary solvent system: acetonitrile (solvent A) and water containing 50 mmol/L ammonium acetate (solvent B). The initial solvent composition was 100% A. 100% A was maintained for 3 min, decreasing from the initial conditions to 50% A within 8.0 min, holding for 4 min before returning to the initial state at 12.0 min, and allowing 4 min for column re-equilibration. The total run time was 16 min, injection-to-injection. The flow rate was 0.3 mL/min. The mass spectrometer ionization source settings were optimized for maximum precursor ion yields for each metabolite. This was achieved by infusing a 1 μg/mL methanolic solution of each individual compound.[47] The following transitions were monitored for the metabolites of interest: glucose 6-phosphate (G6P) 259.00 > 96.90, cone 40 V and collision energy 13 eV; glyceraldehyde 3-phosphate (G3P) 168.90 > 96.90, cone 40 V and collision energy 6 eV; phosphoenolpyruvate (PEP) 166.90 > 78.90, cone 40 V and collision energy 7 eV; lactate (L) 89.00 > 43.00, cone 40 V and collision energy 6 eV; malate (M) 133.00 > 115.00, cone 40 V and collision energy 8 eV. The capillary voltage was 3.00 kV, source temperature was 100 °C, desolvation temperature was 400 °C, and collision cell gas pressure was 3.5×10^{-3} mbar argon. The interchannel and interscan delay times were 0.02 and 0.10 s, respectively. The dwell time was 0.200 s for each analyte. The P value was calculated by applying Student's t-test. NADP+/NADPH was determined in 10^5 cell pellets, obtained as previously described, for each sample at 565 nm by an ultrasensitive colorimetric kit (EnzyChromTM NADP +/NADPH Assay Kit, BioAssay Systems). p value was calculated by applying Student's t-test.

Western Blotting

Transduced CSCs were collected by centrifugation at 1200 rpm. Cell pellets were washed twice with ice-cold PBS, resuspended in a 50 mM Tris-HCl, pH 7.5, 150 mM NaCl, 1 mM EDTA, 1 mM NaF, 10% glycerol, 1 mM MgCl, 1% Triton X-100 ice-cold buffer containing proteinase inhibitor cocktail (Sigma-Aldrich), and incubated for 30′ on ice. Lysates were centrifuged at 10 000g for 10′ and supernatants were collected. 2.5 μg of cell extracts were resolved on a 12% SDS-polyacrylamide gel using a mini-gel apparatus (Bio-Rad Laboratories). Western blots were performed as previously described[48] by using the following antibodies: anti-lactate dehydrogenase (PA5-27406, Thermo Scientific), anti-PKM2 (PA-23034, Thermo Scientific), anti-G6PD (PA5-27359, Thermo Scientific), anti-p63 (clone Y4A3, P3362, Sigma-Aldrich), anti-β-Actin (clone AC-15, A5441 Sigma-Aldrich).

RESULTS

Quantitative Proteomics by Stable Isotope Dimethyl Labeling and Functional Analysis of Modulated Proteins

To evaluate the effect of p63 isoforms expression on cellular processes, we employed a quantitative proteomic study. Colon CSCs derived from a primary tumor as previously described[28] were transduced with lentiviral vectors carrying either TA or ΔNp63. Prior to proteomic analysis, TAp63α and ΔNp63α expression were evaluated in cell extracts obtained 48 h postinfection (Figure 1). Then, protein extracts of colon CSCs

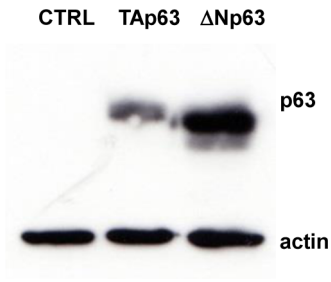

Figure 1. Evaluation of αp63 expression 48 h postinfection. Representative experiment of Western blotting showing the level of TAp63α and ΔNp63α expression after 48 h of infection. Actin was used as loading control.

transduced with empty vector, CTRL, and with vectors overexpressing TAp63α or ΔNp63α were digested by trypsin prior reaction with dimethyl labels. We employed an off line 2-D peptide separation strategy using IEF in the first step. The labeled samples were mixed and loaded on 18 cm immobiline dry strip, pH 3–10 NL, for peptides separation. The focused

dx.doi.org/10.1021/pr4012574 | J. Proteome Res. 2014, 13, 2120–2136

Table 1. List of Modulated Proteins Identified by Chemical Quantitative Analysis in TAp63 Cells with Respect to Control Cells

accession[a]	description[b]	score[c]	mass[d]	TAp63/CTRL[e]	SD(geo)[f]	#[g]
AK1BA_HUMAN	aldo-keto reductase family 1 member B10	105	37283	0.35	1.05	2
AK1C1_HUMAN	aldo-keto reductase family 1 member C1	70	38055	0.35	1.01	2
HSP71_HUMAN	heat shock 70 kDa protein 1A/1B	518	71696	0.36	1.36	6
METK2_HUMAN	S-adenosylmethionine synthase isoform type-2	78	44841	0.4		1
LEG4_HUMAN	galectin-4	268	36397	0.43		1
CH10_HUMAN	10 kDa heat shock protein	476	11233	0.49	1.54	5
CAPG_HUMAN	macrophage-capping protein	86	39529	0.52		1
NPM_HUMAN	nucleophosmin	417	33651	0.52	1.44	3
EF1G_HUMAN	elongation factor 1-gamma	282	51455	0.53		1
IPYR_HUMAN	inorganic pyrophosphatase	140	33880	0.53		1
KCRB_HUMAN	creatine kinase B-type	302	43491	0.54	1.13	2
CH60_HUMAN	60 kDa heat shock protein	1432	62886	0.6	1.10	9
ECH1_HUMAN	delta(3,5)-delta(2,4)-dienoyl-CoA isomerase	300	36612	0.6		1
ETFA_HUMAN	electron transfer flavoprotein subunit alpha	162	36129	0.6		1
UGDH_HUMAN	UDP-glucose 6-dehydrogenase	648	56683	0.6	1.12	5
PRDX1_HUMAN	peroxiredoxin-1	298	22857	0.61		1
HSPB1_HUMAN	heat shock protein beta-1	586	23022	0.62	1.08	5
MDHM_HUMAN	malate dehydrogenase	702	36666	0.62	1.19	8
ECHM_HUMAN	enoyl-CoA hydratase	169	32496	0.63		1
H33_HUMAN	histone H3.3	122	15740	0.63	1.32	4
IF4A1_HUMAN	eukaryotic initiation factor 4A-I	132	46913	0.63	1.25	2
K1C19_HUMAN	keratin, type I cytoskeletal 19	678	44472	0.63	1.13	5
TKT_HUMAN	transketolase	581	69696	0.63	1.07	7
HNRPQ_HUMAN	heterogeneous nuclear ribonucleoprotein Q	61	71077	0.67		1
ADT2_HUMAN	ADP/ATP translocase 2	341	33704	0.68	1.42	4
HNRPK_HUMAN	heterogeneous nuclear ribonucleoprotein K	554	51846	0.68	1.12	4
GRP75_HUMAN	stress-70 protein	659	75378	0.69	1.27	3
AGR2_HUMAN	anterior gradient protein 2 homologue	106	20528	0.69	1.48	3
DHSA_HUMAN	succinate dehydrogenase	317	74485	0.69	1.32	2
HSP7C_HUMAN	heat shock cognate 71 kDa protein	1004	72596	0.69	1.33	7
LMNA_HUMAN	prelamin-A/C	487	75501	0.69	1.38	6
H2A2A_HUMAN	histone H2A type 2-A	769	14479	1.32	1.23	10
SERA_HUMAN	D-3-phosphoglycerate dehydrogenase	46	58189	1.33		1
PPIB_HUMAN	peptidyl-prolyl cis−trans isomerase B	164	24513	1.35	1.30	4
1433T_HUMAN	14-3-3 protein theta	347	28564	1.36		1
TCPD_HUMAN	T-complex protein 1 subunit delta	173	59494	1.36	1.12	2
FLNA_HUMAN	filamin-A	553	287786	1.43		1
GANAB_HUMAN	neutral alpha-glucosidase AB	219	108128	1.45	1.10	2
TBB5_HUMAN	tubulin beta chain	993	50576	1.48		1
PUR6_HUMAN	multifunctional protein ADE2	138	48772	1.48		1
WDR1_HUMAN	WD repeat-containing protein 1	110	67957	1.51		1
IQGA1_HUMAN	Ras GTPase-activating-like protein	142	194057	1.52		1
RLA1_HUMAN	60S acidic ribosomal protein P1	144	11845	1.54		1
SPTN1_HUMAN	spectrin alpha chain	275	290713	1.63		1
H2B1C_HUMAN	histone H2B type 1-C/E/F/G/I	358	14458	1.65		1
UBA1_HUMAN	ubiquitin-like modifier-activating enzyme 1	440	120343	1.69		1
HNRPL_HUMAN	heterogeneous nuclear ribonucleoprotein L	124	65533	1.71		1
DHX9_HUMAN	ATP-dependent RNA helicase A	174	144264	1.85		1
RS10_HUMAN	40S ribosomal protein S10	68	19250	2.44		1
NDUAD_HUMAN	NADH dehydrogenase [ubiquinone] 1	58	16880	3.52		1
CSPG4_HUMAN	chondroitin sulfate proteoglycan	104	251996	4.54		1

[a]ID protein according to SwissProt database. [b]Protein description. [c]Mascot score. Only proteins identified with score >40 were reported. [d]Protein mass. [e]Protein ratio TAp63/CTRL, expressed as median. Only proteins with a ratio >1.3 and <0.7 are reported. [f]SD (geo) = geometric standard deviation calculated by Distiller; when absent the number of peptides was insufficient to calculate it. [g]Number of peptides used for quantitation. Underlined proteins indicated proteins validated in targeted label free experiment.

strips were cut in several pieces, and extracted peptides were analyzed by nLC−MS/MS for protein identification and quantification. The list of proteins modulated after TAp63 overexpression is reported in Table 1 (See Table 2S in the Supporting Information for peptide identification details). A total of 51 proteins were found differentially regulated with ratio above 1.3 or below 0.7, with peptides satisfying the quality parameters reported in the Experimental Section (Figure 2).

dx.doi.org/10.1021/pr4012574 | J. Proteome Res. 2014, 13, 2120−2136

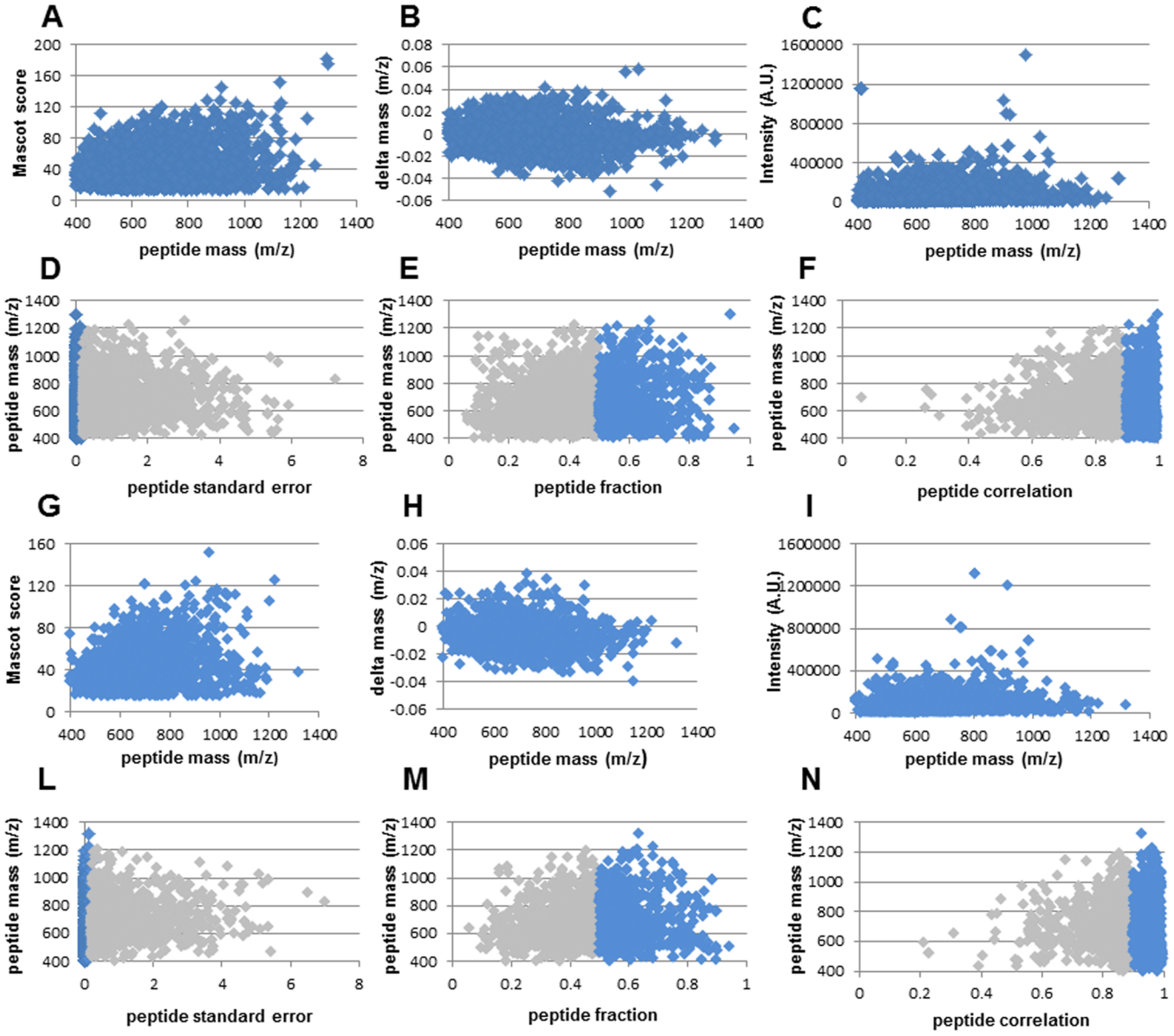

Figure 2. Peptides data quality evaluation for TAp63 (A–F) and ΔNp63 (G–H) data sets. Bar charts showing peptide identification results: Mascot score (A,G), experimental mass error (B,H), and intensity distribution (C,I). Moreover quality parameters for peak detection are displayed: Standard error (D, L), fraction (E,M), and correlation (F,N). (See the Experimental Section for more details.) Gray points represent discarded peptides.

Reported proteins were identified with Mascot score above 40 and FDR < 1%. In the case of ΔNp63 transfected cells, after data processing and database search a total of 38 proteins were found modulated with ratio above 1.3 or below 0.7, whose peptides satisfied the quality parameters reported in the Experimental Section (Figure 2). All reported proteins were identified with Mascot score above 40 and FDR < 1% (Table 2 and Table 3S in the Supporting Information).

Proteins listed in Tables 1 and 2 were used as input files for PANTHER Classification System to classify the biological processes regulated by the proteins modulated in TAp63 and ΔNp63 data set, respectively (Figure 3). As shown in pie charts, apoptosis is the discriminating biological process between the two data sets. NAD-dehydrogenase (NDUAD, GRIM-19), annotated as apoptotic inducers in Panther database, was found to be up-regulated in TAp63 over-expressing cells, whereas galectin-4 (LEG4) and heterogeneous nuclear ribonucleoprotein K (HNRPK), also associated with induction of apoptosis process, were found down-regulated. Interestingly, in both data sets a great part of the modulated proteins was involved in metabolic process, representing 35.1 and 30.3% of the pie chart in TAp63 and ΔNp63 experiments, respectively. Moreover, in both cases, proteins associated with the generation of precursor metabolites and energy were highlighted, underlining the possible involvement of both p63 isoforms in regulating cancer cells metabolism. Proteins included in this biological process were found to be down-regulated after transfection with TAp63 expressing vector. They were: UDP-glucose 6-dehydrogenase (UGDH) involved in biosynthesis of glycosaminoglycans, mitochondrial succinate dehydrogenase (DHSA) and mitochondrial malate dehydrogenase (MDHM) belonging to tricarboxylic acid (TCA) cycle, and mitochondrial electron transfer flavoprotein subunit alpha (ETFA), which transfers electrons to the main mitochondrial respiratory chain. In the ΔNp63 data set, proteins associated with this biological process, ATP-citrate synthase (ACLY) and

dx.doi.org/10.1021/pr4012574 | J. Proteome Res. 2014, 13, 2120–2136

Table 2. List of Modulated Proteins Identified by Chemical Quantitative Analysis in ΔNp63 Cells with Respect to Control Cells

accession[a]	description[b]	score[c]	mass[d]	ΔNp63/CTRL[e]	SD(geo)[f]	#[g]
CLIC1_HUMAN	chloride intracellular channel protein 1	137	27825	0.21		1
HSP71_HUMAN	heat shock 70 kDa protein 1A/1B	577	71696	0.36		1
AK1BA_HUMAN	aldo-keto reductase family 1	76	37150	0.46		1
MIF_HUMAN	macrophage migration inhibitory factor	42	12735	0.48		1
S100P_HUMAN	protein S100-P	52	10731	0.53		1
PTBP1_HUMAN	polypyrimidine tract-binding protein 1	233	58282	0.60	1.35	3
EZRI_HUMAN	ezrin	58	71247	0.62		1
METK2_HUMAN	*S*-adenosylmethionine synthase	46	44732	0.64		1
RL30_HUMAN	60S ribosomal protein L30	136	13396	0.66		1
CH10_HUMAN	10 kDa heat shock protein	280	11277	0.67	1.43	5
G6PI_HUMAN	glucose-6-phosphate isomerase	424	64316	0.68	1.10	4
RL5_HUMAN	60S ribosomal protein L5	88	35550	0.69		1
KCRB_HUMAN	creatine kinase B-type	179	43491	0.70		1
FAS_HUMAN	fatty acid synthase	696	278602	1.30	1.03	5
GSTP1_HUMAN	glutathione *S*-transferase P	128	23905	1.31	1.35	3
ARP3B_HUMAN	actin-related protein 3B	51	48764	1.32		1
ACTN4_HUMAN	alpha-actinin-4	515	106870	1.32		1
MDHC_HUMAN	malate dehydrogenase	139	37500	1.39		1
LPPRC_HUMAN	leucine-rich PPR motif-containing protein	60	162272	1.40		1
SAHH_HUMAN	adenosylhomocysteinase	62	49185	1.40		1
HNRPF_HUMAN	heterogeneous nuclear ribonucleoprotein F	149	46433	1.40		1
HYOU1_HUMAN	hypoxia up-regulated protein 1	232	113963	1.42		1
PPIB_HUMAN	peptidyl-prolyl cis−trans isomerase B	93	24618	1.42		1
ACLY_HUMAN	ATP-citrate synthase	47	123982	1.42		1
ANXA5_HUMAN	annexin A5	159	36677	1.43		1
RS14_HUMAN	40S ribosomal protein S14	48	16867	1.52		1
K1C18_HUMAN	keratin, type I cytoskeletal 18	487	48617	1.53	1.39	6
IPYR_HUMAN	inorganic pyrophosphatase	76	33993	1.62		1
CALX_HUMAN	calnexin	128	69524	1.62		1
HSP74_HUMAN	heat shock 70 kDa protein 4	84	97723	1.63		1
K1C19_HUMAN	Keratin, type I cytoskeletal 19	302	44472	1.69		1
WDR1_HUMAN	WD repeat-containing protein 1	61	68118	1.86		1
EF1D_HUMAN	elongation factor 1-delta	70	31777	1.90		1
PELP1_HUMAN	proline-, glutamic acid-, and leucine-rich protein 1	48	121440	1.95		1
MATR3_HUMAN	matrin-3	53	96928	2.12		1
HSP7C_HUMAN	heat shock cognate 71 kDa	536	72596	2.16		1
CSPG4_HUMAN	chondroitin sulfate proteoglycan 4	192	251880	2.22	1.24	2

[a]ID protein according to SwissProt database. [b]Protein description. [c]Mascot score. Only protein identified with score >40 were reported. [d]Protein mass. [e]Protein ratio ΔNp63/CTRL, expressed as median. Only protein with a ratio >1.3 and <0.7 are reported. [f]SD (geo) = geometric standard deviation calculated by Distiller; when absent the number of peptides was insufficient to calculate it. [g]Number of peptides used for quantitation. Underlined proteins indicated proteins validated in targeted label free experiment.

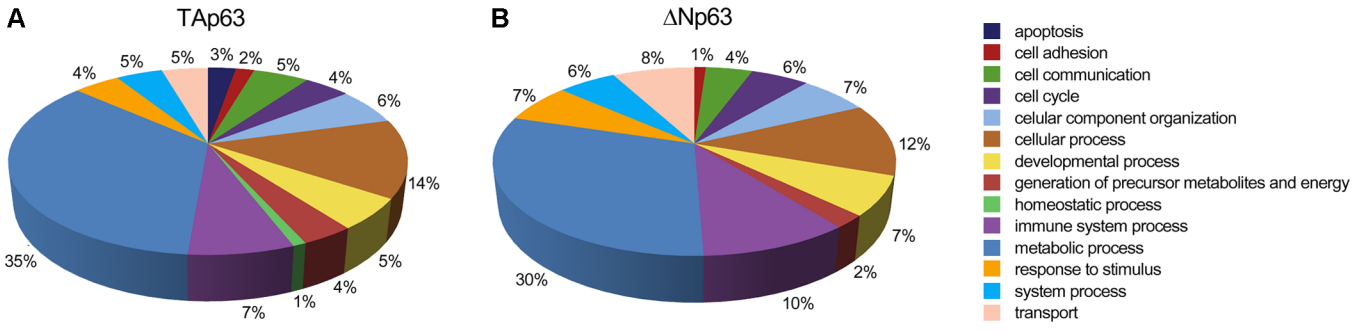

Figure 3. Functional analysis by PANTHER classification system. Pie charts showing biological processes of modulated proteins found in TAp63 (A) and ΔNp63 (B).

cytoplasmic malate dehydrogenase (MDHC), were found to be up-regulated in transfected cells. In mitochondria, ACLY uses acetyl-CoA and oxaloacetate to produce citrate, which is transported to the cytosol. Here citrate is used by citrate lyase to generate acetyl-CoA, while the resulting oxaloacetate is converted to malate by cytoplasmic MDH, thus producing NADPH. The observed modulation of both ACLY and cytoplasmic MDH suggested an increased production of

dx.doi.org/10.1021/pr4012574 | J. Proteome Res. 2014, 13, 2120−2136

acetyl-CoA, which can be used in lipid synthesis. Moreover fatty acid synthetase (FAS) was found to be up-regulated in ΔNp63 expressing cells.

Molecular and cellular functions were investigated also by Ingenuity Pathway Analysis software (IPA) (Table 3). Results

Table 3. Ingenuity Pathway Analysis Results: List of Significant Molecular and Cellular Function

molecular and cellular function	*p* value	no. of molecules
TAp63 Experiment		
cellular assembly and organization	3.06×10^{-6} to 4.73×10^{-2}	15
energy production	8.94×10^{-6} to 2.10×10^{-2}	7
nucleic acid metabolism	8.94×10^{-6} to 3.28×10^{-2}	11
small-molecule metabolism	8.94×10^{-6} to 4.62×10^{-2}	20
post-translational modification	8.87×10^{-5} to 2.69×10^{-2}	8
ΔNp63 Experiment		
cell death and survival	6.45×10^{-6} to 4.05×10^{-2}	21
cellular function and maintenance	8.73×10^{-5} to 4.16×10^{-2}	13
cell cycle	1.79×10^{-4} to 4.78×10^{-2}	13
cell morphology	1.79×10^{-4} to 4.29×10^{-2}	10
cellular assembly and organization	1.79×10^{-4} to 4.04×10^{-2}	16

emphasized the perturbation of metabolic process and process associated with cellular assembly and organization in TAp63 experiment and cell death and survival, cellular function and maintenance, cell cycle, cell morphology, and cellular assembly and organization in ΔNp63 experiment.

Performing functional annotation cluster by DAVID in TAp63 data set, functions associated with stress response and protein folding were enriched in cluster 1 with a score of 3.55 (Table 4S in the Supporting Information). Interestingly the second ranked cluster was prevalently associated with mitochondrion and organelle lumen (enrichment score = 3.19), thus indicating alterations of mitochondrial processes after TAp63 expression. In particular, NADH dehydrogenase (NDUAD), creatine kinase (KKRB), ETFA, enoyl coenzyme A hydratase (ECHM), four heat shock proteins (CH10, CH60, HSP71, and GRP75), MDHM, peroxiredoxin 1 (PRDX1), solute carrier family 25 (ADT2, ADP/ATP translocase 2), and DHSA were associated with mitochondrion in cluster 2. Submitting ΔNp63 data set to DAVID, the enriched Cluster 1, with score of 2.83, was mostly composed of proteins associated with stress response, heat shock proteins, ATP, or nucleoside binding, indicating the modulation of energy metabolism and nucleic acid metabolism after ΔNp63 expression (Table 5S in the Supporting Information).

To investigate TAp63- and ΔNp63-mediated cellular signaling, we performed an unsupervised bioinformatics analysis using IPA. Known mutual interactions among differentially expressed proteins were used to construct protein networks ranked by score (Table 4). In the TAp63 experiment, the network generated with higher score and associated with energy production, nucleic acid metabolism, and small molecule biochemistry functions (Figure 4A) was constructed by some of

Table 4. Ingenuity Pathway Analysis Results: List of Significant Networks

network	associated network functions	score
TAp63 Experiment		
1	energy production, nucleic acid metabolism, small-molecule biochemistry	58
2	developmental disorder, hereditary disorder, metabolic disease	29
3	tissue morphology, cell morphology, hematological system development and function	21
ΔNp63 Experiment		
1	cancer, tumor morphology, cell death and survival	51
2	RNA post-transcriptional modification, post-translational modification, carbohydrate metabolism	27
3	hematological disease, hereditary disorder, tissue morphology	13

the already cited proteins, such as heat shock proteins, CKRB, ECHM, MDHM, PRDX1, ADT2 (SLC25A5), and UGDH. The main nodes deduced by IPA were represented by Akt and MAPK1/2, which are known to be essential for glucose homeostasis.[49] Network with higher score in ΔNp63 experiment was associated with cancer, tumor morphology, cell death, and survival (Figure 2B). Relevant modulated proteins of this network were: heat shock proteins, structural proteins such as keratins (K1C18), actinin 4 (ACTN4), and actin-binding protein, which is associated with cell motility and cancer metastasis,[50] ezrin (EZR), involved in maintaining the cell cortex,[51] and enzymes, such as CKRB and glucose-6-phosphate isomerase (G6PI, GPI in the network). Interestingly, the main node of the network deduced by the software was Akt, thus underlining similarity with TAp63. Similarly to TAp63, metabolism was also reported as a relevant network function, although with lower score (score = 27), associated with carbohydrate metabolism, RNA post-transcriptional modification, and post-translational modification in network 2 (Table 3). In silico analysis allowed us to highlight also possible upstream regulators of the reported networks. In both TAp63 and ΔNp63 experiment, Myc was predicted to be modulated with significant score (Figure 5A). Moreover, in the case of ΔNp63 in addition to Myc, also p53 was predicted to be modulated (Figure 5B).

Targeted Label-Free Quantitative Analysis

To validate experimental evidence found by quantitative labeled proteomic investigation followed by in silico functional analysis, we carried out a targeted label-free strategy to quantify the proteotypic peptides of regulated proteins of interest. Whole protein extracts of CTRL, TAp63, and ΔNp63-transfected cells were digested by trypsin and loaded on a nanoACQUITY UPLC system coupled to a Q-TOF mass spectrometer operating in high−low mode. Triplicates were run for each condition. Raw data were first analyzed to evaluate chromatographic reproducibility and processed by PLGS software, using SwissProt database restricted to *Homo sapiens* taxonomy, to evaluate the number of total identified proteins. (Representative protein lists identified in a single run of each condition, with FPR < 1%, are reported in Table 6S in the Supporting Information.) The EMRT (exact mass retention time) peptide clusters, that is, the list of paired exact masses and retention times[42−44] found by the software, showed RSD (relative standard deviation) mass below 15 ppm and %CV RT (coefficient variation on retention time) mostly below 6%,

dx.doi.org/10.1021/pr4012574 | J. Proteome Res. 2014, 13, 2120−2136

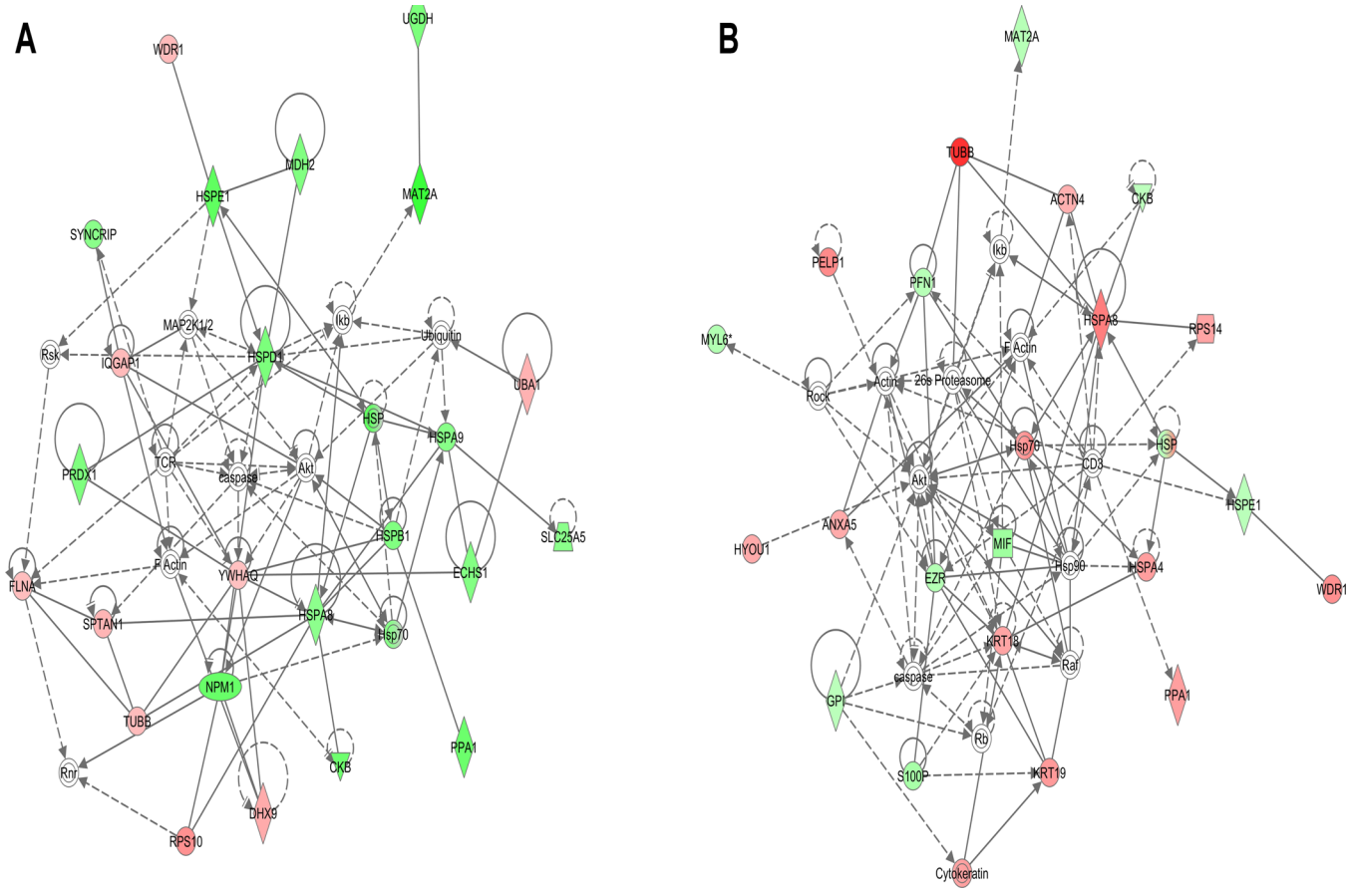

Figure 4. Pathway analysis. (A) Network generated for TAp63 experiment, showing score = 58, was involved in energy production, nucleic acid metabolism, and small-molecule biochemistry. (B) Network with higher score in ΔNp63 experiment was associated with cancer, tumor morphology, cell death, and survival. Nodes represent proteins: shaded features describe proteins identified in the present study (red, up-regulated; green, down-regulated), whereas unshaded features describe additional members deduced by the software.

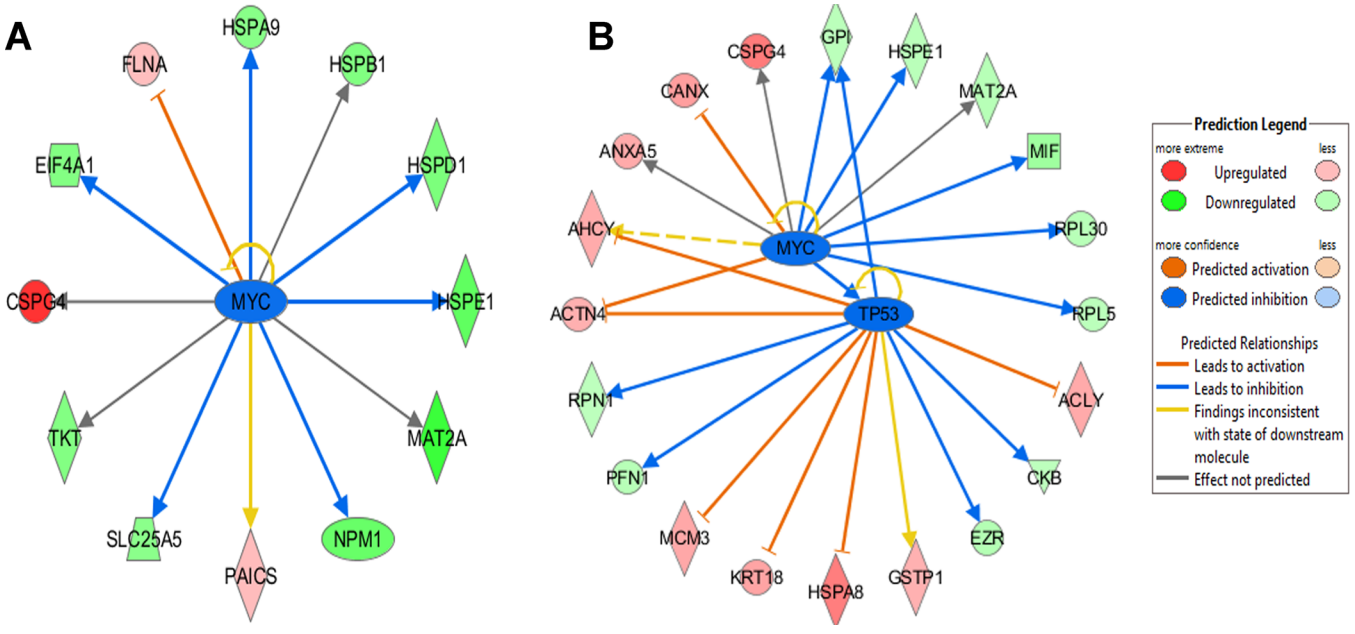

Figure 5. Upstream regulators predicted by in silico analysis. In TAp63, Myc was predicted to be modulated with significant p value = 3.07×10^{-7} (A), while in ΔNp63 experiment, Myc and p53 were predicted to be modulated, p value = 4.23×10^{-7} and 3.65×10^{-6} (B).

and %CV intensity (coefficient variation of EMRTs intensities) showed Gaussian distributions centered on mean value of ~2% CV under the three conditions (Figure 1S in the Supporting Information). Raw data were then used to generate extracted

dx.doi.org/10.1021/pr4012574 | J. Proteome Res. 2014, 13, 2120−2136

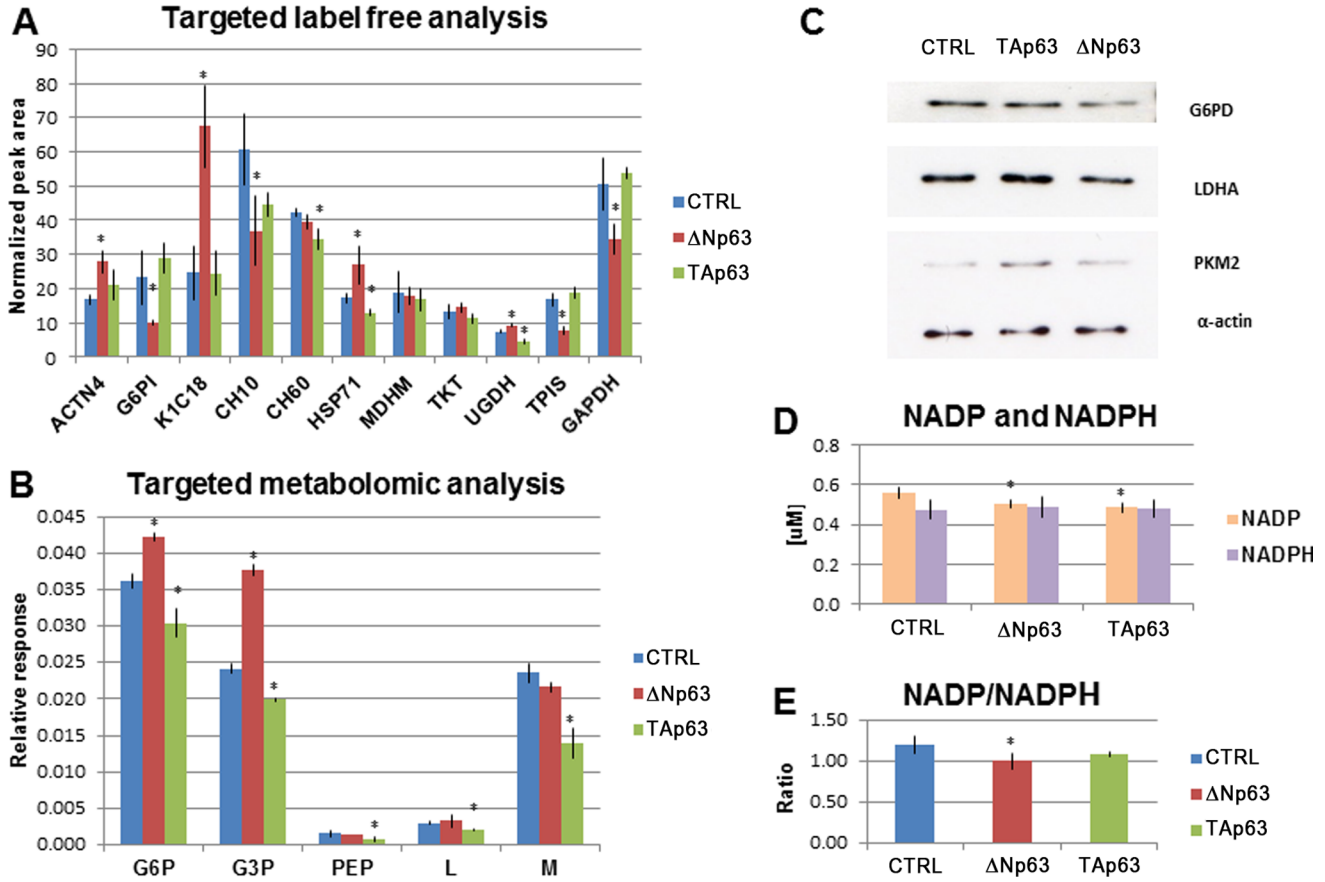

Figure 6. (A) Targeted proteomic analysis. LC−MS/MS runs of unlabeled samples were processed by Skyline software to quantify proteotypic peptides of interesting proteins. ACTN4, alpha actinin 4; CH10, 10 kDa heat shock protein, mitochondrial; CH60, 60 kDa heat shock protein, mitochondrial; HSP71, heat shock 70 kDa protein 1A/1B; G6PI, glucose-6-phosphate isomerase; TPIS, triosephosphate isomerase; GAPDH, glyceraldehyde-3-phosphate dehydrogenase; cytoskeletal keratin-18 (K1C18); mitochondrial malate dehydrogenase (MDHM), UDP-glucose 6-dehydrogenase (UGDH). Protein abundance is reported as peaks area generated by XIC after normalization. Endogenous actin was used as standard for normalization. Error bars represent standard deviation calculated on three different analytical runs. Asterisks indicate statistical significance (*t* test *p* value < 0.05 for TAp63 or ΔNp63 cells vs control cells). More details are reported in Table 5. (B) Targeted metabolomics analysis. Metabolites were extracted from CTRL, TAp63, and ΔNp63 cells. Glucose 6-phosphate (G6P), glyceraldehyde 3-phosphate (G3P), phosphoenolpyruvate (PEP), lactate (L), and malate (M) were determined by mass spectrometry and reported as relative response (arbitrary units, calculated as the peak area of each analyte normalized to the total chromatographic peak areas). Error bars represent standard deviation calculated on three different analytical runs. Asterisks indicate statistical significance (*p* value< 0.05 *t* test of TAp63 or ΔNp63 cells vs control cells.) (C) Immunoblotting analysis. Western-blotting analysis was carried out using whole cell lysate from CTRL, TAp63, and ΔNp63 cells and antibodies against LDHA (lactate dehydrogenase A chain), G6PD (glucose-6-phosphate 1-dehydrogenase), and PKM2 (pyruvate kinase). Actin was used as loading control. (D) Measurement of NADP and NADPH. Asterisks indicate statistical significance (*p* value< 0.05 *t* test of TAp63 or ΔNp63 cells vs control cells). (E) Determination of NADP/NADPH ratio. Asterisks indicate statistical significance (*p* value< 0.05 *t* test of TAp63 or ΔNp63 cells vs control cells).

ion chromatograms (XICs) by Skyline software. XIC traces of MS1 traces were used for integrating peak area and determining the abundance of proteotypic peptides of interesting proteins with respect to actin proteotypic peptides, used for normalization. The following proteins were included in this investigation: mitochondrial heat shock proteins (HSP10, HSP60, and HSP71), alpha actinin 4 (ACTN4), cytokeratin-18 (K1C18), and some metabolic enzymes, such as glucose-6-phosphate isomerase (G6PI), mitochondrial malate dehydrogenase (MDHM), UDP-glucose 6-dehydrogenase (UGDH), triosephosphate isomerase (TPIS), glyceraldehyde-3-phosphate dehydrogenase (GAPDH), and transketolase (TKT) (Figure 6A. Proteins were quantified using two proteotypic peptides (with the exception of CH10, HSP71, and UGDH), with a percentage of coefficient of variation (%CV) for peptide retention times (RTs) below 5% and a %CV calculated for normalized peak area below 30% or close to this value (Table 5). Enolase from *S. cerevisiae* (ENO1) and human enolase alpha (ENOA) were used as control proteins, whose abundance is not expected to be modulated. ENO1 was added as standard in samples prior to acquisition (see the Experimental Section), while ENOA was not found among the significant modulated proteins in both ΔNp63 and TAp63 data sets. Mitochondrial heat shock proteins (HSP10, HSP60, and HSP71), included in mitochondrion and organelle lumen cluster by DAVID analysis and represented among the modulated nodes in network 1 of IPA analysis in TAp63 experiment, were confirmed to be down-regulated with respect to CTRL condition by targeted label-free experiment. Down-regulation of HSP10 was also confirmed for ΔNp63 experiment. UGDH and MDHM, reported in network 1 of TAp63 IPA analysis and members of the PANTHER biological process called generation of precursor metabolites and energy, were found to be down-regulated in TAP63 by labeled approach. These enzymes showed a decrement with respect to control cells also in the targeted analysis, although the trend was more evident in the case of UGDH rather than in

dx.doi.org/10.1021/pr4012574 | *J. Proteome Res.* 2014, 13, 2120−2136

Table 5. Targeted Label-Free Analysis

			RT		CTRL		ΔNp63		TAp63		ΔNp63/CTRL		TAp63/CTRL	
protein ID[a]	peptide sequence[b]	m/z[c]	mean[d]	%CV[e]	peaks area[f]	%CV[g]	peaks area[h]	%CV[i]	peaks area[j]	%CV[k]	ratio[l]	p value[m]	ratio[n]	p value[m]
ACTN4	EAILAIHK	447.77	47.6	2.6	16.9	21.3	27.9	11.8	21.2	21.1	**1.7**	**0.017**	1.3	0.266
	QFASQANVVGPWIQTK	887.47	81.8	1.3										
K1C18	AQIFANTVDNR	660.33	56.2	2.1	24.6	31.7	67.4	17.7	24.4	26.1	**2.7**	**0.032**	0.99	0.096
	AQYDELAR	483.23	42.5	2.7										
G6PI	TLAQLNPESSLFIIASK	916.51	104.2	0.9	23.1	33.1	10.1	6.3	28.9	14.9	0.4	0.098	1.2	0.344
	ILLANFLAQTEALMR	852.48	131.5	0.6										
CH10	VLLPEYGGTK	538.80	61.3	1.2	1.9	17.1	37.0	27.7	44.6	8.2	**0.6**	**0.047**	0.7	0.101
CH60	GYISPYFINTSK	695.36	77.7	1.4	42.2	2.7	39.5	5.3	34.4	8.7	0.9	0.137	**0.8**	**0.033**
	LSDGVAVLK	451.27	54.6	2.2										
HSP71	NQVALNPQNTVFDAK	829.93	69.1	1.6	17.4	8.2	27.0	20.5	13.1	5.5	**1.6**	**0.086**	**0.8**	**0.019**
MDHM	ANTFVAELK	496.77	61.6	2.9	19.5	31.1	17.9	14.1	16.8	19.7	0.9	0.79	0.8	0.61
	TIIPLISQCTPK	685.88	79.9	1.3										
UGDH	VLIGGDETPEGQR	685.84	49.4	2.4	24.6	4.1	9.3	4.4	4.5	13.8	**1.2**	**0.03**	**0.6**	**0.008**
TKT	ILATPPQEDAPSVDIANIR	1010.53	69.9	1.5	13.3	17.1	14.4	10.5	11.2	11.7	1.08	0.5	0.84	0.26
	SVPTSTVFYPSDGVATEK	942.96	80.4	1.3										
TPIS	VPADTEVVCAPPTAYIDFAR	1096.54	92.8	4.4	16.8	12.1	7.80	17.1	18.86	9.1	**0.8**	**0.004**	1.1	0.253
	IIYGGSVTGATCK	663.84	49.7	2.5										
GAPDH	IISNASCTTNCLAPLAK	917.46	65.2	3.2	50.5	15.4	30.4	13.0	53.7	3.2	**0.7**	**0.049**	1.1	0.559
	GALQNIIPASTGAAK	706.40	69.8	1.6										
	VTLTSEEEAR	567.79	39.8	3.1										
ENO1[o]	AVDDFLISLDGTANK	789.90	93.83	1.1	46.4	2.8	45.9	7.0	40.7	11.2	0.99	0.84	0.89	0.20
	IGSEVYHNLK	580.30	42.67	2.9										
	VNQIGTLSESIK	644.85	62.86	1.8										
ENOA[o]	YISPDQLADLYK	713.37	86.06	1.04	207.3	28.65	181.8	8.9	190.4	16.6	0.88	0.61	0.91	0.48

[a]Protein name by SwissProt: ACTN4, alpha actinin 4; CH10, 10 kDa heat shock protein, mitochondrial; CH60, 60 kDa heat shock protein, mitochondrial; HSP71, heat shock 70 kDa protein 1A/1B; G6PI, glucose-6-phosphate isomerase; TPIS, triosephosphate isomerase; GAPDH, glyceraldehyde-3-phosphate dehydrogenase; K1C18, cytoskeletal keratin-18; MDHM, mitochondrial malate dehydrogenase; UGDH, UDP-glucose 6-dehydrogenase; ENO1, enolase from *S. cerevisiae;* ENOA, alpha-enolase. [b]Aminoacidic sequences of peptides used for quantitation. [c]Mass/charge of peptides used for quantitation. [d]Mean of peptide retention time recorded in the replicate runs (expressed in minutes). [e]%CV = coefficient of variation of the peptide retention time expressed as percentage. [f]Normalized peak area of the protein using actin as standard. The value indicates the relative abundance of the protein in replicates of CTRL. [g]Coefficient of variation of the peak area expressed as percentage calculated in CTRL replicates. [h]Normalized peak area of the protein using actin as standard. The value indicates the relative abundance of the protein in replicates of ΔNp63. [i]Coefficient of variation of the peak area expressed as percentage calculated in ΔNp63 replicates. [j]Normalized peak area of the protein using actin as standard. The value indicates the relative abundance of the protein in replicates of TAp63. [k]Coefficient of variation of the peak area expressed as percentage calculated in TAp63, respectively. [l]Ratio of the peak area in ΔNp63 versus CTRL, [m]p value obtained by Student's t test. Significant values are in bold. [n]Ratio of the peak area in TAp63 versus CTRL, respectively. [o]Proteins expected to be not modulated and used as control.

dx.doi.org/10.1021/pr401257t | J. Proteome Res. 2014, 13, 2120−2136

MDHM. TKT, belonging to pentose phosphate pathway (PPP), was found to be decreased in label-free analysis in TAp63 overexpressing cells, as already observed by labeled approach. Trends of ACTN4, K1C18, and G6PI, included in network 1 of ΔNp63, were also confirmed in this validating phase: ACTN4 and K1C18 showed a marked increment in ΔNp63, whereas G6PI was decreased with respect to control condition.

Targeted Metabolomics Analysis

To better characterize the metabolic state of TAp63 and ΔNp63 expressing cells, we performed a targeted metabolomics analysis, evaluating the cellular relative abundance of five relevant metabolites for the reported biochemical pathways by monitoring their mass spectrometry transitions: glucose 6-phosphate (G6P), glyceraldehyde 3-phosphate (G3P), phosphoenolpyruvate (PEP), lactate (L), and malate (M) (Figure 6B). Results showed significant accumulation of G6P and G3P in ΔNp63 cells, while these metabolites were less abundant in TAp63 cells, with respect to control condition. Accumulation of substrates of the first steps of glycolysis, such as G6P and G3P, was associated with decreased levels of G6PI, TPIS, and GAPDH in ΔNp63 cells. G6PI was found to be down-regulated by both labeled and unlabeled proteomic analysis, while TPIS and GAPDH were reported only for the label-free proteomic strategy, although in the labeled approach TPIS showed a fold change of 0.8 with respect to control conditions, which was omitted in the corresponding table because under the selected threshold for ratio. These results may be indicative of a slower rate of the first steps of glycolysis under this condition with respect to control cells. In anaerobic glycolysis, lactate dehydrogenase (LDHA) reduces pyruvate to produce lactate (L), using NAD as coenzyme. In ΔNp63 cells, a significant increment of L was not observed by targeted metabolomics analysis, and insignificant modulation of LDHA protein was detected (Figure 6C). Moreover, in these cells, we did not detect a modulation in protein level of pyruvate kinase (PKM2) (Figure 6C), a key regulatory enzyme of glycolytic pathway that catalyzes the transfer of a phosphate group from PEP to ADP, yielding one molecule of pyruvate and one molecule of ATP. Furthermore, PPP may be less favored in ΔNp63-expressing cells, as indicated by the down-regulation of glucose-6-phospate-dehydrogenase (G6PD), the enzyme controlling the rate-limiting step of PPP, as observed by Western blotting experiment (Figure 6C), and by the decrement of NADP/NADPH ratio, which was caused by reduced NADP availability rather than enhanced NADPH production (Figure 6D,E). In TAp63 overexpressing cells, the decrease in G6P and G3P was accompanied by moderate up-regulation of G6PI and GAPDH, observed in both proteomic approaches (although the fold change of 1.22 for GAPDH was not reported in Table 1 because it was under the threshold fixed for ratio) and TPIS only in label-free approach, underlining a possible opposite effect of the two p63 isoforms on glycolysis. Glycolysis may be accelerated in TAp63, as also indicated by up-regulation of PKM2, detected by Western blotting (Figure 6C), which rapidly converts PEP to pyruvate. Unlike ΔNp63 cells, under TAp63 condition PEP, L and M were significantly less abundant with respect to control. LDHA was lightly up-regulated, while modulation of G6PD was not detected in TAp63 cells by Western blotting (Figure 6C). The NADP/NADPH ratio was approximately the same as that determined in control cells (Figure 6D,E). Interestingly, the reduced amount of malate, a TCA intermediate, was associated with the reduced levels of two TCA cycle enzymes, such as succinate dehydrogenase (DHSA), reported only in labeled proteomic analysis, and MDHM, in both labeled and label-free proteomic analysis.

DISCUSSION

On the basis of the knowledge of p63's role in the regulation of epithelial cell stemness and differentiation, it is reasonable to suspect that it may also play a role in regulating the phenotypic characteristics of CSCs through the control of several molecular pathways, including self-renewal and differentiation processes.[23] Recent studies reported that ΔNp63 isoforms can regulate the mRNA expression and splicing of CD44, a surface glycoprotein marking CSCs in various epithelial tumors including HNSCC and breast cancer.[52] ΔNp63α induces a stem-cell phenotype in the MCF7 breast cancer cell line, and it has been suggested that it could be a marker of breast CSC.[53] Recently, it was reported that ΔNp63-positive cells embody the stem/progenitor properties in prostate, bladder, and colorectal epithelium, providing a potential source of cells that can differentiate into neoplastic cells.[19]

In this study, we used CSCs isolated from colon, overexpressing TAp63α or ΔNp63α, to evaluate cellular signaling mediated by the two isoforms, following a quantitative labeled proteomic strategy, coupled to functional in silico analysis.

A substantial number of proteins modulated by both p63 isoforms belong to cellular assembly and organization and to cellular morphology, among which there are also proteins involved in tumor progression and metastasis. Chondroitin sulfate proteoglycan 4, CSPG4, a surface protein that is known to modulate oligodendrocyte precursor cells migration[54] and to be associated with invasiveness in glioma and melanoma tumors,[55] was found increased in both TAp63- and ΔNp63-expressing cells. Other structural proteins involved in cellular migration were found up-regulated, such as filamin-A (FLNA) in TAp63 and actinin-4 (ACTN4) in ΔNp63, respectively. FLNA is an actin-binding protein playing an essential role in cytoskeletal plasticity and flexibility to respond to environmental stimuli by interacting with extracellular matrix (ECM) components.[56] FLNA also interacts with many metastasis-related proteins, and its inhibition may reduce this process, although the mechanism of action remains not completely clarified.[57] ACTN4 is a component of focal adhesion, protein complexes that mediate cell migration by physically connecting the ECM to the cytoskeleton.[58] These findings suggested the involvement of p63 in metastatic process of CSCs, as already observed in other cellular model of cancer.[11,14]

Interestingly a significant portion of modulated proteins, reported in this work, were involved in metabolic processes. A common distinct feature of cancer cells is the so-called "aerobic glycolysis", which consists of enhanced lactate production, originally known as Warburg effect.[59] However, metabolic rearrangement is not limited to glycolysis but also involves the TCA cycle, β-oxidation, and anabolic metabolism in general by furnishing not only energy but also components for the synthesis of nucleotides and amino and fatty acids to sustain cellular growth and survival.[60] In the recent years, it is becoming clear that different key cellular signals guide the metabolic adaptation of tumor cells, such as hypoxia inducible factor-1 (HIF-1) and PI3K/Akt/mTOR pathways, oncogenes such as c-Myc, and tumor suppressor such as p53.[61] Under hypoxia condition, HIF-1 activates the transcription of genes

encoding glucose transporters and most glycolytic enzymes, increasing the glycolytic activity of cells. Moreover, by activating pyruvate dehydrogenase kinases (PDKs), which inhibits mitochondrial pyruvate dehydrogenase complex, HIF-1 reduces pyruvate flux into the TCA cycle, thus decreasing oxidative phosphorylation and oxygen consumption.[61] The oncogene c-Myc activates glucose transporters, glycolytic enzymes, LDHA and PDK1, and genes involved in mitochondrial biogenesis and function, such as those associated with glutamine metabolism.[61] Activation of PI3K/Akt/mTOR pathway leads to enhanced glycolytic activity by both elevated synthesis of glucose transporters and activation of HIF-1, which cooperates with c-Myc to induce metabolic adaptation in cancer cells.[61] Finally, p53 takes part in the regulation of glucose metabolism, acting on enzymes involved in glycolysis, TCA cycle, glutaminolysis, and PPP.[61] In particular, p53 directly inactivates G6PD, thus inhibiting PPP, while mutated p53 is unable to perform this function, thus causing the increased consumption of glucose, typical of tumor cells.[62] On the contrary, TAp73, but not ΔNp73, promotes biosynthesis and antioxidant protection through the induction of G6PD expression.[58] Moreover, overexpression of TAp73α in human osteosarcoma SAOS-2 promotes PPP process.[64] Flores and colleagues demonstrated that TAp63 regulates several metabolic pathways, through which it may establish its tumor suppressor functions.[65] Mice knockout of TAp63 became obese, accumulating lipid deposits in several tissues. This phenotype can be explained by an increased fatty acid synthesis associated with a concomitant decrease in fatty acid consumption. Moreover, these mice also developed defects in glucose metabolism. Furthermore, TAp63−/− mouse embryonic fibroblasts (MEFs) showed a slower rate of mitochondrial oxidative phosphorylation, which is a peculiar metabolic alteration of cancer cells, and reduced glucose uptake, which, on the contrary, is in contrast with that observed in tumor cells.[65]

In this study, the in silico functional analysis highlighted the modulation of cellular signaling responsible for metabolic adaptation in the cancer cell, such as c-Myc and PI3K/Akt/mTOR, in both TAp63- and ΔNp63-overexpressing cells, and p53, only in ΔNp63-expressing cells. Proteins and metabolites of glycolysis were modulated in TAp63- and ΔNp63-expressing cells but with opposite trends. In TAp63-overexpressing cells the level of glycolytic intermediates determined by targeted analysis was significantly inferior to that observed in control cells. In parallel, we observed the increased levels of glycolytic enzymes, such as G6PI, TPIS, GAPDH, and PKM2. G6PI, which catalyzes the second step of the glycolysis by the reversible isomerization of glucose-6-phosphate into fructose-6-phosphate, is an essential enzyme involved in catabolic glycolysis, anabolic gluconeogenesis, and it is known to influence tumor cell growth.[60] Deficiency of TPIS, another essential glycolytic enzyme, is associated with nonspherocytic hemolytic anemia and a severe neurological disorder, while its up-regulation has been reported in several cancers, including lung, liver, colon, breast, bone, and prostate.[60] Onco-proteomics studies showed that also GAPDH is overexpressed in various neoplasias.[60] In addition to glycolysis, GAPDH is involved in different biological functions, such as DNA repair and telomeric DNA binding, transcriptional regulation, membrane fusion, RNA binding, tubulin assembly, and apoptosis induction.[60] Pyruvate kinase (PK) is a key regulatory enzyme, catalyzing an irreversible reaction of the glycolysis. L, R, M1, and M2 are the four PK isoenzymes in mammals. Among them, the PKM2 isoenzyme is preferentially expressed in tumor cells.[60] G6PI, TPIS, and GAPDH are significantly down-regulated in ΔNp63-expressing cells. Also, G6PD was detected in lower quantity in ΔNp63 as compared with control and TAp63 conditions. Moreover, the down-regulation of TCA cycle enzymes, such as DHSA and MDHM, and the lower level of malate may be suggestive of a perturbed mitochondrial oxidative phosphorylation in TAp63- expressing cells. Modulation of other proteins associated with mitochondrion, such as HSP10, HSP60, and HSP71, was indicative of an altered function of this organelle, particularly in TAp63-expressing cells.

Mitochondria play a key role not only in energy production but also in the cross-talk of metabolic pathways and signals for apoptosis and autophagy.[66,67] Mitochondrial functions are carried out by continuous signal exchanges both from nucleus to mitochondrion, anterograde signaling, and from mitochondrion to nucleus, retrograde signaling.[66] An example of retrograde signaling is represented by the mitochondrial unfolded protein response, originated from the efflux of peptides from damaged mitochondrial matrix proteins to the cytosol, which is mediated by mitochondrial HSPs. Mitochondrial chaperones promote protein folding and proteases that degrade misfolded proteins, leading to more efficient mitochondrial function and biogenesis.[68]

The cross-talk of the mitochondrial proteins with the nuclear encoded proteins is a fundamental task of Mitochondrial Proteome Initiative (mt-HPP),[68] which will strictly cooperate with the Biology/Disease Human Proteome Project (B/D-HPP),[69] one of the most recent initiatives launched by the Human Proteome Organization. The present study provides initial evidence toward dissecting p63 functions in CSCs, although additional studies are required to go deeper inside this issue to achieve new insight into the signaling pathways beyond the differences in metabolism response correlated to TAp63 or ΔNp63 expression. Nevertheless, evidence described here could be matter of debate inside the scientific community involved in both mt-HPP and B/D-HPP.

In conclusion, in this work, we employed a proteomic study, by both labeled and unlabeled approaches, coupled to bioinformatics and targeted metabolomics analysis to dissect the intracellular pathways triggered by TAp63 or ΔNp63 isoforms in human CSCs line isolated from colon cancer. Our results indicate that p63 is implicated in a wide range of biological processes, including metabolism. Interestingly, TAp63-overexpressing cells are more glycolytic active than ΔNp63 cells, indicating that the two isoforms may regulate the key steps of glycolysis in an opposite manner. Further investigations are necessary to elucidate the underlying molecular mechanisms determining glycolysis regulation by TAp63 and ΔNp63 isoforms.

■ ASSOCIATED CONTENT

Supporting Information

Supplementary Table 1S: Peptides identification of D0 and D2 samples. Supplementary Table 2S: Peptide table of differentially expressed proteins identified in TAp63 data set. Supplementary Table 3S: Peptide table of differentially expressed proteins identified in ΔNp63 data set. Supplementary Table 4S: Cluster Analysis by DAVID for TAp63 data set. Supplementary Table 5S: Cluster Analysis by DAVID for ΔNp63 data set.

dx.doi.org/10.1021/pr4012574 | J. Proteome Res. 2014, 13, 2120−2136

Supplementary Table 6S: Protein identified by label-free MS^e analysis. Supplementary Table 7S: spectra of proteins identified with single peptide. Figure 1S: Data quality evaluation of label-free MS^e analysis reproducibility. This material is available free of charge via the Internet at http://pubs.acs.org.

AUTHOR INFORMATION

Corresponding Authors

*A.U.: E-mail: andrea.urbani@uniroma2.it.
*V.D.L.: E-mail: delaurenzi@unich.it.

Author Contributions

∇A.U. and V.D.L. have been acting as senior investigators and should be considered equal last authors.

Notes

The authors declare no competing financial interest.

ACKNOWLEDGMENTS

V.D.L. was supported by grant AIRC 11450 and Ministero Sanita' Finalizzata 2009. A.U. was supported by MIUR grant RBAP11WCRZ_003. We thank the PRIDE team (http://www.ebi.ac.uk/pride) for helpful assistance in mass spectrometry data uploading.

REFERENCES

(1) Levrero, M.; De Laurenzi, V.; Costanzo, A.; Gong, J.; Wang, J. Y.; Melino, G. The p53/p63/p73 family of transcription factors: overlapping and distinct functions. *J. Cell Sci.* **2000**, *113* (Pt 10), 1661−1670.

(2) De Laurenzi, V.; Melino, G. Evolution of functions within the p53/p63/p73 family. *Ann. N.Y. Acad. Sci.* **2000**, *926*, 90−100.

(3) Muller, P. A.; Vousden, K. H. p53 mutations in cancer. *Nat. Cell Biol.* **2013**, *15* (1), 2−8.

(4) Allocati, N.; Di Ilio, C.; De Laurenzi, V. p63/p73 in the control of cell cycle and cell death. *Exp. Cell Res.* **2012**, *318* (11), 1285−1290.

(5) Candi, E.; Dinsdale, D.; Rufini, A.; Salomoni, P.; Knight, R. A.; Mueller, M.; Krammer, P. H.; Melino, G. TAp63 and DeltaNp63 in cancer and epidermal development. *Cell Cycle* **2007**, *6* (3), 274−285.

(6) Graziano, V.; De Laurenzi, V. Role of p63 in cancer development. *Biochim. Biophys. Acta* **2011**, *1816* (1), 57−66.

(7) Nylander, K.; Vojtesek, B.; Nenutil, R.; Lindgren, B.; Roos, G.; Zhanxiang, W.; Sjöström, B.; Dahlqvist, A.; Coates, P. J. Differential expression of p63 isoforms in normal tissues and neoplastic cells. *J Pathol.* **2002**, *198* (4), 417−427.

(8) Su, X.; Chakravarti, D.; Flores, E. R. p63 steps into the limelight: crucial roles in the suppression of tumorigenesis and metastasis. *Nat Rev Cancer.* **2013**, *13* (2), 136−143.

(9) Di Como, C. J.; Urist, M. J.; Babayan, I.; Drobnjak, M.; Hedvat, C. V.; Teruya-Feldstein, J.; Pohar, K.; Hoos, A.; Cordon-Cardo, C. p63 expression profiles in human normal and tumor tissues. *Clin. Cancer Res.* **2002**, *8* (2), 494−501.

(10) Higashikawa, K.; Yoneda, S.; Tobiume, K.; Saitoh, M.; Taki, M.; Mitani, Y.; Shigeishi, H.; Ono, S.; Kamata, N. DeltaNp63alpha-dependent expression of Id-3 distinctively suppresses the invasiveness of human squamous cell carcinoma. *Int J Cancer.* **2009**, *124* (12), 2837−2844.

(11) Tucci, P.; Agostini, M.; Grespi, F.; Markert, E. K.; Terrinoni, A.; Vousden, K. H.; Muller, P. A.; Dötsch, V.; Kehrloesser, S.; Sayan, B. S.; Giaccone, G.; Lowe, S. W.; Takahashi, N.; Vandenabeele, P.; Knight, R. A.; Levine, A. J.; Melino, G. Loss of p63 and its microRNA-205 target results in enhanced cell migration and metastasis in prostate cancer. *Proc Natl Acad Sci U S A.* **2012**, *109* (38), 15312−15317.

(12) Su, X.; Chakravarti, D.; Cho, M. S.; Liu, L.; Gi, Y. J.; Lin, Y. L.; Leung, M. L.; El-Naggar, A.; Creighton, C. J.; Suraokar, M. B.; Wistuba, I.; Flores, E. R. TAp63 suppresses metastasis through coordinate regulation of Dicer and miRNAs. *Nature* **2010**, *467* (7318), 986−90.

(13) Gressner, O.; Schilling, T.; Lorenz, K.; Schulze Schleithoff, E.; Koch, A.; Schulze-Bergkamen, H.; Lena, A. M.; Candi, E.; Terrinoni, A.; Catani, M. V.; Oren, M.; Melino, G.; Krammer, P. H.; Stremmel, W.; Müller, M. TAp63alpha induces apoptosis by activating signaling via death receptors and mitochondria. *EMBO J.* **2005**, *24* (13), 2458−2471.

(14) Melino, G. p63 is a suppressor of tumorigenesis and metastasis interacting with mutant p53. *Cell Death Differ.* **2011**, *18* (9), 1487−1499.

(15) Yang, A.; Schweitzer, R.; Sun, D.; Kaghad, M.; Walker, N.; Bronson, R. T.; Tabin, C.; Sharpe, A.; Caput, D.; Crum, C.; McKeon, F. p63 is essential for regenerative proliferation in limb, craniofacial and epithelial development. *Nature* **1999**, *398* (6729), 714−718.

(16) Mills, A. A.; Zheng, B.; Wang, X. J.; Vogel, H.; Roop, D. R.; Bradley, A. p63 is a p53 homologue required for limb and epidermal morphogenesis. *Nature* **1999**, *398* (6729), 708−713.

(17) Karni-Schmidt, O.; Castillo-Martin, M.; Shen, T. H.; Gladoun, N.; Domingo-Domenech, J.; Sanchez-Carbayo, M.; Li, Y.; Lowe, S.; Prives, C.; Cordon-Cardo, C. Distinct expression profiles of p63 variants during urothelial development and bladder cancer progression. *Am. J. Pathol.* **2011**, *178* (3), 1350−1360.

(18) Romano, R. A.; Smalley, K.; Magraw, C.; Serna, V. A.; Kurita, T.; Raghavan, S.; Sinha, S. ΔNp63 knockout mice reveal its indispensable role as a master regulator of epithelial development and differentiation. *Development* **2012**, *139* (4), 772−82.

(19) Pignon, J. C.; Grisanzio, C.; Geng, Y.; Song, J.; Shivdasani, R. A.; Signoretti, S. p63-expressing cells are the stem cells of developing prostate, bladder, and colorectal epithelia. *Proc Natl Acad Sci U S A.* **2013**, *110* (20), 8105−8110.

(20) Senoo, M.; Pinto, F.; Crum, C. P.; McKeon, F. p63 is essential for the proliferative potential of stem cells in stratified epithelia. *Cell* **2007**, *129* (3), 523−536.

(21) Koster, M. I.; Dai, D.; Marinari, B.; Sano, Y.; Costanzo, A.; Karin, M.; Roop, D. R. p63 induces key target genes required for epidermal morphogenesis. *Proc Natl Acad Sci U S A.* **2007**, *104* (9), 3255−60.

(22) Su, X.; Paris, M.; Gi, Y. J.; Tsai, K. Y.; Cho, M. S.; Lin, Y. L.; Biernaskie, J. A.; Sinha, S.; Prives, C.; Pevny, L. H.; Miller, F. D.; Flores, E. R. TAp63 prevents premature aging by promoting adult stem cell maintenance. *Cell Stem Cell.* **2009**, *5* (1), 64−75.

(23) Nekulova, M.; Holcakova, J.; Coates, P.; Vojtesek, B. The role of p63 in cancer, stem cells and cancer stem cells. *Cell Mol Biol Lett.* **2011**, *16* (2), 296−327.

(24) O'Brien, C. A.; Pollett, A.; Gallinger, S.; Dick, J. E. A human colon cancer cell capable of initiating tumour growth in immunodeficient mice. *Nature* **2007**, *445* (7123), 106−110.

(25) Ricci-Vitiani, L.; Lombardi, D. G.; Pilozzi, E.; Biffoni, M.; Todaro, M.; Peschle, C.; De Maria, R. Identification and expansion of human colon-cancer-initiating cells. *Nature* **2007**, *445* (7123), 111−115.

(26) Todaro, M.; Francipane, M. G.; Medema, J. P.; Stassi, G. Colon cancer stem cells: promise of targeted therapy. *Gastroenterology* **2010**, *138* (6), 2151−2162.

(27) Scatena, R.; Bottoni, P.; Giardina, B. Circulating tumour cells and cancer stem cells: a role for proteomics in defining the interrelationships between function, phenotype and differentiation with potential clinical applications. *Biochim. Biophys. Acta* **2013**, *1835* (2), 129−143.

(28) Todaro, M.; Alea, M. P.; Di Stefano, A. B.; Cammareri, P.; Vermeulen, L.; Iovino, F.; Tripodo, C.; Russo, A.; Gulotta, G.; Medema, J. P.; Stassi, G. Colon cancer stem cells dictate tumor growth and resist cell death by production of interleukin. *Cell Stem Cell* **2007**, *4* (1), 389−402.

(29) Candi, E.; Rufini, A.; Terrinoni, A.; Dinsdale, D.; Ranalli, M.; Paradisi, A.; De Laurenzi, V.; Spagnoli, L. G.; Catani, M. V.; Ramadan, S.; Knight, R. A.; Melino, G. Differential roles of p63 isoforms in

epidermal development: selective genetic complementation in p63 null mice. *Cell Death Differ.* **2006**, *13* (6), 1037−1047.
(30) Ricci-Vitiani, L.; Pedini, F.; Mollinari, C.; Condorelli, G.; Bonci, D.; Bez, A.; Colombo, A.; Parati, E.; Peschle, C.; De Maria, R. Absence of caspase 8 and high expression of PED protect primitive neural cells from cell death. *J Exp Med.* **2004**, *200* (10), 1257−66.
(31) Follenzi, A.; Ailles, L. E.; Bakovic, S.; Geuna, M.; Naldini, L. Gene transfer by lentiviral vectors is limited by nuclear translocation and rescued by HIV-1 pol sequences. *Nat. Genet.* **2000**, *25* (2), 217−222.
(32) Boersema, P. J.; Raijmakers, R.; Lemeer, S.; Mohammed, S.; Heck, A. J. Multiplex peptide stable isotope dimethyl labeling for quantitative proteomics. *Nat Protoc.* **2009**, *4* (4), 484−494.
(33) Hsu, J. L.; Huang, S. Y.; Chow, N. H.; Chen, S. H. Stable-isotope dimethyl labeling for quantitative proteomics. *Anal. Chem.* **2003**, *75* (24), 6843−6852.
(34) Boutilier, J. M.; Warden, H.; Doucette, A. A.; Wentzell, P. D. Chromatographic behaviour of peptides following dimethylation with H2/D2-formaldehyde: implications for comparative proteomics. *J Chromatogr B Analyt Technol Biomed Life Sci.* **2012**, *1* (908), 59−66.
(35) Levi Mortera, S.; Dioni, I.; Greco, V.; Neri, C.; Rovero, P.; Urbani. A.; pH-regulated formation of side products in the reductive amination approach for differential labeling of peptides in relative quantitative experiments. *Electrophoresis* **2014**, *00*, 1−9.in press.
(36) De Canio, M.; D'Aguanno, S.; Sacchetti, C.; Petrucci, F.; Cavagni, G.; Nuccetelli, M.; Federici, G.; Urbani, A.; Bernardini, S. Novel IgE recognized components of Lolium perenne pollen extract: comparative proteomics evaluation of allergic patients sensitization profiles. *J Proteome Res.* **2009**, *8* (9), 4383−4391.
(37) Chick, J. M.; Haynes, P. A.; Molloy, M. P.; Bjellqvist, B.; Baker, M. S.; Len, A. C. Characterization of the rat liver membrane proteome using peptide immobilized pH gradient isoelectric focusing. *J Proteome Res.* **2008**, *7* (3), 1036−1045.
(38) Cantor, D.; Slapetova, I.; Kan, A.; McQuade, L. R.; Baker, M. S. Overexpression of *αvβ6* integrin alters the colorectal cancer cell proteome in favor of elevated proliferation and a switching in cellular adhesion that increases invasion. *J Proteome Res.* **2013**, *12* (6), 2477−2490.
(39) Mendes, M.; Pérez-Hernandez, D.; Vázquez, J.; Coelho, A. V.; Cunha, C. Proteomic changes in HEK-293 cells induced by hepatitis delta virus replication. *J Proteomics.* **2013**, *89*, 24−38.
(40) Vizcaíno, J. A.; Côté, R. G.; Csordas, A.; Dianes, J. A.; Fabregat, A.; Foster, J. M.; Griss, J.; Alpi, E.; Birim, M.; Contell, J.; O'Kelly, G.; Schoenegger, A.; Ovelleiro. D.; Pérez-Riverol, Y.; Reisinger, F.; Ríos, D.; Wang, R.; Hermjakob, H. The PRoteomics IDEntifications (PRIDE) database and associated tools: status in 2013. *Nucleic Acids Res.* **2013**, *41*(Database issue):D1063−9. doi: 10.1093/nar/gks1262.
(41) Côté, R. G.; Griss, J.; Dianes, J. A.; Wang, R.; Wright, J. C.; van den Toorn, H. W.; van Breukelen, B.; Heck, A. J.; Hulstaert, N.; Martens, L.; Reisinger, F.; Csordas, A.; Ovelleiro, D.; Perez-Rivevol, Y.; Barsnes, H.; Hermjakob, H.; Vizcaíno, J. A. The PRoteomics IDEntification (PRIDE) Converter 2 framework: an improved suite of tools to facilitate data submission to the PRIDE database and the ProteomeXchange consortium. *Mol Cell Proteomics.* **2012**, *11* (12), 1682−1689.
(42) D'Aguanno, S.; D'Alessandro, A.; Pieroni, L.; Roveri, A.; Zaccarin, M.; Marzano, V.; De Canio, M.; Bernardini, S.; Federici, G.; Urbani, A. New insights into neuroblastoma cisplatin resistance: a comparative proteomic and meta-mining investigation. *J Proteome Res.* **2011**, *10* (2), 416−428.
(43) D'Alessandro, A.; D'Aguanno, S.; Cencioni, M. T.; Pieroni, L.; Diamantini, A.; Battistini, L.; Longone, P.; Spalloni, A.; De Laurenzi, V.; Bernardini, S.; Federici, G.; Urbani, A. Protein repertoire impact of Ubiquitin-Proteasome System impairment: insight into the protective role of beta-estradiol. *J Proteomics.* **2012**, *75* (4), 1440−1453.
(44) D'Aguanno, S.; D'Agnano, I.; De Canio, M.; Rossi, C.; Bernardini, S.; Federici, G.; Urbani, A. Shotgun proteomics and network analysis of neuroblastoma cell lines treated with curcumin. *Mol Biosyst.* **2012**, *8* (4), 1068−1077.
(45) MacLean, B.; Tomazela, D. M.; Shulman, N.; Chambers, M.; Finney, G. L.; Frewen, B.; Kern, R.; Tabb, D. L.; Liebler, D. C.; MacCoss, M. J. Skyline: an open source document editor for creating and analyzing targeted proteomics experiments. *Bioinformatics* **2010**, *26* (7), 966−968.
(46) De Canio, M.; Soggiu, A.; Piras, C.; Bonizzi, L.; Urbani, A.; Galli, A.; Roncada, P. Differential protein profile in sexed bovine semen: shotgun proteomics investigation *Mol. Biosyst.* **2013**, Epub ahead of print, DOI: 10.1039/C3MB70306A
(47) Marzano, V.; Santini, S.; Rossi, C.; Zucchelli, M.; D'Alessandro, A.; Marchetti, C.; Mingardi, M.; Stagni, V.; Barilà, D.; Urbani, A. Proteomic profiling of ATM kinase proficient and deficient cell lines upon blockage of proteasome activity. *J Proteomics* **2012**, *75* (15), 4632−4646.
(48) Munarriz, E.; Barcaroli, D.; Stephanou, A.; Townsend, P. A.; Maisse, C.; Terrinoni, A.; Neale, M. H.; Martin, S. J.; Latchman, D. S.; Knight, R. A.; Melino, G.; De Laurenzi, V. PIAS-1 is a checkpoint regulator which affects exit from G1 and G2 by sumoylation of p73. *Mol. Cell. Biol.* **2004**, *24* (24), 10593−10610.
(49) Schultze, S. M.; Hemmings, B. A.; Niessen, M.; Tschopp, O. PI3K/AKT, MAPK and AMPK signalling: protein kinases in glucose homeostasis. *Expert Rev Mol Med.* **2012**, DOI: 10.1017/S1462399411002109.
(50) Koizumi, T.; Nakatsuji, H.; Fukawa, T.; Avirmed, S.; Fukumori, T.; Takahashi, M.; Kanayama, H. The role of actinin-4 in bladder cancer invasion. *Urology* **2010**, *75* (2), 357−364.
(51) Neisch, A. L.; Fehon, R. G. Ezrin, Radixin and Moesin: key regulators of membrane-cortex interactions and signaling. *Curr Opin Cell Biol.* **2011**, *23* (4), 377−382.
(52) Boldrup, L.; Coates, P. J.; Gu, X.; Nylander, K. DeltaNp63 isoforms regulate CD44 and keratins 4, 6, 14 and 19 in squamous cell carcinoma of head and neck. *J. Pathol.* **2007**, *213*, 384−391.
(53) Du, Z.; Li, J.; Wang, L.; Bian, C.; Wang, Q.; Liao, L.; Dou, X.; Bian, X.; Zhao, R. C. Overexpression of ΔNp63*α* induces a stem cell phenotype in MCF7 breast carcinoma cell line through the Notch pathway. *Cancer Sci.* **2010**, *101*, 2417−2424.
(54) Binamé, F.; Sakry, D.; Dimou, L.; Jolivel, V.; Trotter, J. NG2 regulates directional migration of oligodendrocyte precursor cells via Rho GTPases and polarity complex proteins. *J. Neurosci.* **2013**, *33* (26), 10858−1074.
(55) Campoli, M.; Ferrone, S.; Wang, X. Functional and clinical relevance of chondroitin sulfate proteoglycan 4. *Adv. Cancer Res.* **2010**, *109*, 73−121.
(56) Yue, J.; Huhn, S.; Shen, Z. Complex roles of filamin-A mediated cytoskeleton network in cancer progression. *Cell Biosci.* **2013**, *3* (1), 7 DOI: 10.1186/2045-3701-3-7.
(57) Jiang, X.; Yue, J.; Lu, H.; Campbell, N.; Yang, Q.; Lan, S.; Haffty, B. G.; Yuan, C.; Shen, Z. Inhibition of filamin-A reduces cancer metastatic potential. *Int J Biol Sci.* **2013**, *9* (1), 67−77.
(58) Hamill, K. J.; Hopkinson, S. B.; Skalli, O.; Jones, J. C. Actinin-4 in keratinocytes regulates motility via an effect on lamellipodia stability and matrix adhesions. *FASEB J.* **2013**, *27* (2), 546−556.
(59) Warburg, O. On the origin of cancer cells. *Science* **1956**, *123*, 309−314.
(60) Scatena, R.; Bottoni, P.; Pontoglio, A.; Giardina, B. Revisiting the Warburg effect in cancer cells with proteomics. The emergence of new approaches to diagnosis, prognosis and therapy. *Proteomics Clin Appl.* **2010**, *4* (2), 143−158.
(61) Cairns, R. A.; Harris, I. S.; Mak, T. W. Regulation of cancer cell metabolism. *Nat Rev Cancer.* **2011**, *11* (2), 85−95.
(62) Jiang, P.; Du, W.; Wang, X.; Mancuso, A.; Gao, X.; Wu, M.; Yang, X. p53 regulates biosynthesis through direct inactivation of glucose-6-phosphate dehydrogenase. *Nat. Cell Biol.* **2011**, *13* (3), 310−316.
(63) Du, W.; Jiang, P.; Mancuso, A.; Stonestrom, A.; Brewer, M. D.; Minn, A. J.; Mak, T. W.; Wu, M.; Yang, X. TAp73 enhances the pentose phosphate pathway and supports cell proliferation. *Nat. Cell Biol.* **2013**, *15* (8), 991−1000.

(64) D'Alessandro, A.; Marrocco, C.; Rinalducci, S.; Peschiaroli, A.; Timperio, A. M.; Bongiorno-Borbone, L.; Finazzi Agrò, A.; Melino, G.; Zolla, L. Analysis of TAp73-dependent signaling via omics technologies. *J Proteome Res.* **2013**, *12* (9), 4207−4220.
(65) Su, X.; Gi, Y. J.; Chakravarti, D.; Chan, I. L.; Zhang, A.; Xia, X.; Tsai, K. Y.; Flores, E. R. TAp63 is a master transcriptional regulator of lipid and glucose metabolism. *Cell Metab.* **2012**, *16* (4), 511−525.
(66) Guha, M.; Avadhani, N. G. Mitochondrial retrograde signaling at the crossroads of tumor bioenergetics, genetics and epigenetics. *Mitochondrion.* **2013**, *13* (6), 577−591.
(67) Bottoni, P.; Giardina, B.; Pontoglio, A.; Scarà, S.; Scatena, R. Mitochondrial proteomic approaches for new potential diagnostic and prognostic biomarkers in cancer. *Adv. Exp. Med. Biol.* **2012**, *942*, 423−40.
(68) Urbani, A.; De Canio, M.; Palmieri, F.; Sechi, S.; Bini, L.; Castagnola, M.; Fasano, M.; Modesti, A.; Roncada, P.; Timperio, A. M.; Bonizzi, L.; Brunori, M.; Cutruzzolà, F.; De Pinto, V.; Di Ilio, C.; Federici, G.; Folli, F.; Foti, S.; Gelfi, C.; Lauro, D.; Lucacchini, A.; Magni, F.; Messana, I.; Pandolfi, P. P.; Papa, S.; Pucci, P.; Sacchetta, P. Italian Mt-Hpp Study Group-Italian Proteomics Association (www.itpa.it).The mitochondrial Italian Human Proteome Project initiative (mt-HPP). *Mol Biosyst.* **2013**, *9* (8), 1984−1992.
(69) Aebersold, R.; Bader, G. D.; Edwards, A. M.; van Eyk, J. E.; Kussmann, M.; Qin, J.; Omenn, G. S. The biology/disease-driven human proteome project (B/D-HPP): enabling protein research for the life sciences community. *J Proteome Res.* **2013**, *12* (1), 23.